Part II: Stability and Noise

Chapter 3

Frequency and Intensity Noise of Er-doped Fiber DFB Lasers

Abstract — The relative intensity (RIN) and optical frequency (ν_{rms}) noise of Er-doped fiber DFB lasers are investigated theoretically and experimentally. For a free running 1480-nm pumped fiber DFB laser with 170 μW output power we observe a typical RIN floor of -118 dB Hz$^{-1/2}$ for frequencies above 10 Hz, with a strong relaxation oscillation resonance peak reaching a peak value of -77 dB Hz$^{-1/2}$ at 222 kHz. The measured ν_{rms} ranges from 26 dB Hz/$\sqrt{\text{Hz}}$ at 1 kHz to 2 dB Hz/$\sqrt{\text{Hz}}$ at 1 MHz, with a sharp peak at the relaxation oscillation frequency. Below 1 kHz $1/f$ noise is observed in the laser frequency measurements. Negative feedback to the pump from a monitor detector reduces the RIN to the detection noise level, while the relaxation oscillation noise peak is removed from ν_{rms}. By comparing measured intensity and frequency fluctuations, we estimate the effective linewidth broadening factor at the relaxation oscillation frequencies of the investigated lasers to be between 2.1 and 3.8, as compared to typically between 3 and 7 for semiconductor lasers. The noise performance of four serially multiplexed fiber DFB lasers are found to be similar to that of the free running single lasers.

3.1 Introduction

The accuracy of optical sensors, such as interferometers, fiber Bragg grating sensors and high-resolution spectroscopic sensors, are in many cases limited by the accuracy by which the optical frequency of the interrogating source can be controlled or stabilized. Some of the most accurate sources known on

the market today are ring-cavity Nd:YAG lasers [1] and Er:Yb-doped bulk glass lasers [2, 3]. Compared to single frequency fiber lasers these sources are relatively complicated to maintain and produce. They are also space consuming, and not easily tunable over large frequency ranges.

Fiber lasers can also be used as sensing elements, as demonstrated in [4, 5, 6], as well as in Chapters 7, 8, and 9. The optical pumping and frequency interrogation systems may then be situated far from the sensor lasers. The ultimate sensor accuracy will also in this case be limited by the intrinsic frequency noise of the lasers. It is therefore of interest to investigate the typical noise level of such lasers, and to investigate the origins of this noise in order to identify possible routes towards a further reduction of the noise.

Degrading of sensor accuracy due to source intensity noise can in principle be eliminated, for instance by monitoring the source power on a separate detector or by use of balanced interference detection schemes. However, these techniques tend to complicate the sensor design. Furthermore, parts of the laser frequency noise may actually arise from the intensity noise through thermal effects and the linewidth enhancement factor of the gain medium. Furthermore, It is therefore also of interest to investigate the intensity noise characteristics of the fiber DFB lasers.

This chapter is organized as follows: A theoretical framework for the study of laser noise and noise generating mechanisms is presented in Sec. 3.2. The aspects of thermally and acoustically induced noise in fiber DFB lasers are reviewed in Secs. 3.3 and 3.4, respectively. In Sec. 3.5 we characterize the sensitivity of the intensity and optical frequency of a fiber DFB laser to pump modulation, and we discuss the mechanisms causing this sensitivity. Measurements of the intensity and frequency modulation noise spectra from the lasers are presented in Sec. 3.6, while active noise suppression by applying negative feedback from the fiber laser output to the pump laser drive current is investigated in Sec. 3.7. The noise performance of serially multiplexed fiber DFB lasers is investigated experimentally in Sec. 3.8. Sec. 3.9 contains some concluding remarks.

3.2 Theory

A general theoretical framework for the study of laser intensity and frequency noise can be found in standard textbooks [7]. A purpose of this section is to define parameters and derive relations that can be related directly to the fiber DFB laser parameters.

3.2.1 Definitions of RIN, Frequency Noise, and Laser Linewidth

We let $A(t) = |A(t)| \exp(2\pi\nu(t))$ represent the complex optical field amplitude of the laser output as a function of time t, where $\nu(t) = \nu_0 + \Delta\nu(t) = \nu_0 + d\phi_s/(2\pi dt)$ is the instantaneous laser frequency. ν_0 is the mean laser frequency, while $\Delta\nu(t) = d\phi_s/(2\pi dt)$ represent the time dependent frequency fluctuations. $\phi_s(t)$ is the time-dependent optical phase fluctuations.

The relative fluctuations in the laser output power $P(t) = |A(t)|^2$ is defined as $RI = P(t)/P_o - 1$, where $P_o = \langle P(t) \rangle$ is the mean output power. The operator $\langle \cdot \rangle$ here means taking the average or expectation value. The relative intensity noise $RIN(f)$ (expressed in $\mathrm{Hz}^{-1/2}$) is defined by the relation $RIN^2(f) = \langle |RI^2(f)| \rangle$, which expresses the power spectral density of $RI(t)$ versus the electrical frequency f at which the noise is monitored.

The optical frequency noise $\nu_{rms}(f)$ (expressed in $\mathrm{Hz}/\sqrt{\mathrm{Hz}}$) is defined is defined by the relation $\nu^2_{rms}(f) = \langle |\Delta\nu^2(f)| \rangle$, which expresses the power spectral density of $\Delta\nu(t)$. The phase noise density ϕ_{rms} (expressed in $\mathrm{rad}/\sqrt{\mathrm{Hz}}$) is related to ν_{rms} by $\phi_{rms} = \nu_{rms}/f$.

The power spectral density $|A(\nu)|^2$ of the laser output field depends both on the phase $\phi_{rms}(f)$ and RIN noise spectra of the laser. In most cases, however, $\phi_{rms}(f)$ will dominate over the RIN. From Fourier theory we know that $|A(\nu)|^2$ is the Fourier transform of the auto-correlation function $\langle A(t)A(t+\tau) \rangle$. For the case where the RIN is negligible, Weissman shows in [8] that (for a noise process obeying Gaussian statistics) the auto-correlation function takes the form:

$$\langle A(t)A(t+\tau) \rangle = \left\langle |A(t)|^2 \right\rangle e^{-\Lambda(\tau)/2}, \tag{3.1}$$

where $\Lambda(\tau) = \left\langle [\phi_s(t+\tau) - \phi_s(t)]^2 \right\rangle$ represents the variance of the interference phase that would arise in an interferometer with delay τ.

If we assume ν_{rms} to be independent on f (white noise), $\phi_s(t) = 2\pi \int_0^t (\nu(\hat{t}) - \nu_0) d\hat{t}$ represents a "random walk process". We then find:

$$\begin{aligned} \Lambda(\tau) &= \left\langle [\phi_s(t+\tau) - \phi_s(t)]^2 \right\rangle \\ &= \left\langle \left[\int_t^{t+\tau} 2\pi\nu\left(\hat{t}\right) \, d\hat{t} \right]^2 \right\rangle = 4\pi^2 \tau \nu^2_{rms}. \end{aligned} \tag{3.2}$$

The laser coherence time τ_{coh} is often defined as the interferometer delay time τ for which $\langle A(t)A(t+\tau) \rangle$ has dropped to e^{-2} of its maximum value. (3.1) and (3.2) then implies:

$$\tau_{coh} = (\pi\nu_{rms})^{-2} \tag{3.3}$$

Inserting (3.2) into (3.1) and transforming to the frequency domain results in the following Lorenzian form of $|A(\nu)|^2$:

$$|A(\nu)|^2 = \frac{|A(\nu_0)|^2}{1 + (\nu - \nu_0)^2/\Delta\nu_{3dB}^2}, \tag{3.4}$$

where, $\Delta\nu_{3dB}$ is the laser full-width-half-maximum linewidth, defined as:

$$\Delta\nu_{3dB} = (\pi\tau_{coh})^{-1} = \pi\nu_{rms}^2. \tag{3.5}$$

In practice, (3.4) and (3.5) will produce good approximations for $|A(\nu)|^2$, provided that $\nu_{rms}(f)$ is flat up to a few octaves above $f = \Delta\nu_{3dB}$. More precisely stated: The contributions from deviations from a flat spectrum in $\nu_{rms}(f)$ to the integral $\int_0^\infty (\nu_{rms}(f)/f)^2\, df$ should be negligible.

For a free running fiber laser (without active feedback for intensity stabilization), RIN and frequency noise at the relaxation oscillation frequency f_r will usually lead to sidebands in the optical spectrum $|A(\nu)|^2$ at $\nu = \nu_0 \pm f_r$. For large relaxation oscillation amplitudes ($\gtrsim 10$ % modulation depth), higher order sidebands may also be observed at $\nu = \nu_0 \pm k\, f_r$, ($k = 1, 2, \cdots$). Typically, $f_r = 100 - 500$ kHz for Er^{3+}-doped fiber DFB lasers. If the laser is self pulsing (100 % modulation depth), the effects of RIN on the shape of $|A(\nu)|^2$ will be significant, and (3.4, 3.5) will not be valid.

ν_{rms} will usually increase at low frequencies f due to ambient temperature drift, acoustical vibrations, etc. In semiconductor and solid state (Nd:YAG) lasers, $1/f$ noise processes of less understood origins are also known to play a role. Usually, one does not want to include the long-term frequency drift in the calculation of $\Delta\nu_{3dB}$. One solution to this problem is to maintain the definition $\langle A(t)A(t + \tau_{coh})\rangle = 1/e$ given above for the coherence time τ_{coh}, and use (3.5) as a definition for the 3-dB bandwidth. Alternatively, one may define $\Delta\nu_{3dB}$ as the full-width-half-maximum of $|A(\nu)|^2$ averaged over a specified recording time. With both definitions, ν_0 will be time-dependent on long time-scales.

3.2.2 Classification of Noise Sources

The origins of RIN and laser frequency noise can be classified into four categories:

1. *Spontaneous emission seeding* of the laser operation, represented by a white noise source of spectral power density e_{sp}^2 (W/Hz) radiating into the cavity. The complex field amplitude $e_{sp}(t)$ of the spontaneous emission is added to the existing field $M^{-1/2}A(t)$ in the cavity, where M is the laser mirror transmissivity to the output port. The resulting perturbations of the relative amplitude $RI/2$ and the phase ϕ_s are not correlated, but with equal rms magnitudes $e_{sp}(M/P_o)^{1/2}$. The field perturbations are

integrated over time due to the recirculation in the cavity every roundtrip time τ_{rt}. The field perturbations $d|A|/dt$ and $d\phi_s/dt$ resulting from this integration is called the Langevin force [7].

2. *Optical resonance frequency perturbations* of the cold cavity causing a direct contribution to $\Delta\nu$. By "cold cavity" we mean the cavity, including possible back reflections from the lead fiber, but excluding the effects of the active gain medium. The resonance frequency perturbations may originate from external thermal or mechanical perturbations.

3. *Loss perturbations* of the cold cavity, represented by a modulation Δa_{rt} of the roundtrip loss in absence of active gain (defined more precisely below). Such loss perturbations could originate from random fluctuations in saturable absorber losses, or by randomly varying external back reflections. The loss integrates over time into a RI contribution.

4. *Pump efficiency perturbations*, which may be due to fluctuations in the relative intensity RI_p, center wavelength, or polarization state of the pump. These fluctuations will lead to fluctuations Δg_{rt} in the roundtrip gain contributed from the active gain medium. (Δg_{rt} is defined more precisely below).

The RI and ν_s (or ϕ_s) observed at the output from the laser will generally be different from the input signals discussed above, due to feedback and interactions between the gain, loss, intensity, and resonance frequency. These interactions will be discussed in the following sub-sections.

3.2.3 A Model for the Interaction Between Gain and RI

The small-signal interaction between the active gain medium and the RI can be described by the following rate equations:

$$\begin{aligned} \frac{dRI}{dt} &= \frac{\Delta g_{rt} - \Delta a_{rt} + 2(M/P_o)^{1/2} e_{sp}}{\tau_{rt}} \\ \frac{d\Delta g_{rt}}{dt} &= \tau_{sat}^{-1} \Delta g_{rt} + (k_{slope} RI_p - RI) k_{sat} g_{rt}. \end{aligned} \tag{3.6}$$

Here, g_{rt} is the contribution from the active gain medium to the field amplitude roundtrip gain coefficient of the laser (corresponding to the variable rtg_g in Chap. 6). At steady state we have $g_{rt} = a_{rt}$ where a_{rt} is the cold cavity roundtrip loss. Δg_{rt} and Δa_{rt} are the small-signal deviations of g_{rt} and a_{rt} from steady state.

$\tau_{sat} \equiv \partial \Delta g_{rt}/(\Delta g_{rt} \partial t)$ in (3.6) is the saturated lifetime of the gain medium for the given signal and pump intensities. It is convenient also to introduce the

saturation frequency as $f_{sat} = 1/(2\pi\tau_{sat})$. For a two-level gain medium (like the 1480-nm pumped Er-laser) we have

$$\tau_{sat}^{-1} = 2\pi f_{sat} = \tau_{sp}^{-1} + (\sigma_{se} + \sigma_{sa})P_o/M + (\sigma_{pe} + \sigma_{pa})P_p, \tag{3.7}$$

where τ_{sp}^{-1} is spontaneous and stimulated emission rate, σ_{xy} is the emission ($y = e$) and absorption ($y = a$) cross-sections (normalized with respect to the photon energy and the overlap with the mode cross section area) at the signal ($x = s$) and pump ($x = p$) wavelengths, and P_o/M and P_p are the signal and pump intensities inside the cavity, respectively.

k_{sat} in (3.6) is defined as $k_{sat} \equiv \partial\Delta g_{rt}/\partial RI$ where the differential should be evaluated at DC ($f \to 0$). For our two-level gain medium we have $k_{sat} = (1 + P_{sat}M/P_o)$ where P_{sat} is the saturation power of the gain medium for the given pump power. In the following we will assume that $k_{sat} \simeq 1$, corresponding to $P_o/M \gg P_{sat}$ which is believed to be valid for most fiber DFB lasers. k_{slope} is determined by the slope efficiency of the laser at DC, and is defined as

$$k_{slope} = RI(f \to 0)/RI_p(f \to 0). \tag{3.8}$$

(3.6) can be transformed to the Fourier frequency domain by substituting $i2\pi f$ for d/dt. The resulting small-signal flow diagram is shown in Fig. 3.1 (a). A feedback loop from Δg_{rt} to RI and back to Δg_{rt} can be identified in the figure, with roundtrip transfer function:

$$\begin{aligned} H_0(f) &= \frac{-g_{rt}}{i\pi\tau_{rt}f(1 + if/f_{sat})} \\ &= \frac{-f_r^2 f_{sat}^{-1}}{if(1 + if/f_{sat})}\,. \end{aligned} \tag{3.9}$$

Here,

$$f_r = \sqrt{\frac{g_{rt}f_{sat}}{\pi\tau_{rt}}} \tag{3.10}$$

is the frequency at which $|H_0(f_r)| \simeq 1$. f_r is called the relaxation oscillation frequency. The magnitude and phase of $H_0(f)$ is illustrated in Fig. 3.1 (b) for values of f_{sat} and f_r that are typically expected in Er-doped fiber DFB lasers.

The transfer functions from the input signals RI_p, Δa_{rt}, and e_{sp} in Fig. 3.1 (a) to the output laser RI can be deduced from the flow diagram to be:

$$\begin{aligned} T_p(f) &= \frac{RI}{RI_p} &&= k_{slope}\frac{H_0(f)}{1 - H_0} \\ T_{loss}(f) &= \frac{RI}{\Delta a_{rt}} &&= \frac{-1}{i\pi\tau_{rt}f\,[1 - H_0(f)]} \\ T_{sp}(f) &= \frac{RI}{e_{sp}} &&= -2\,(M/P_o)^{1/2}\,T_{loss}(f)\ . \end{aligned} \tag{3.11}$$

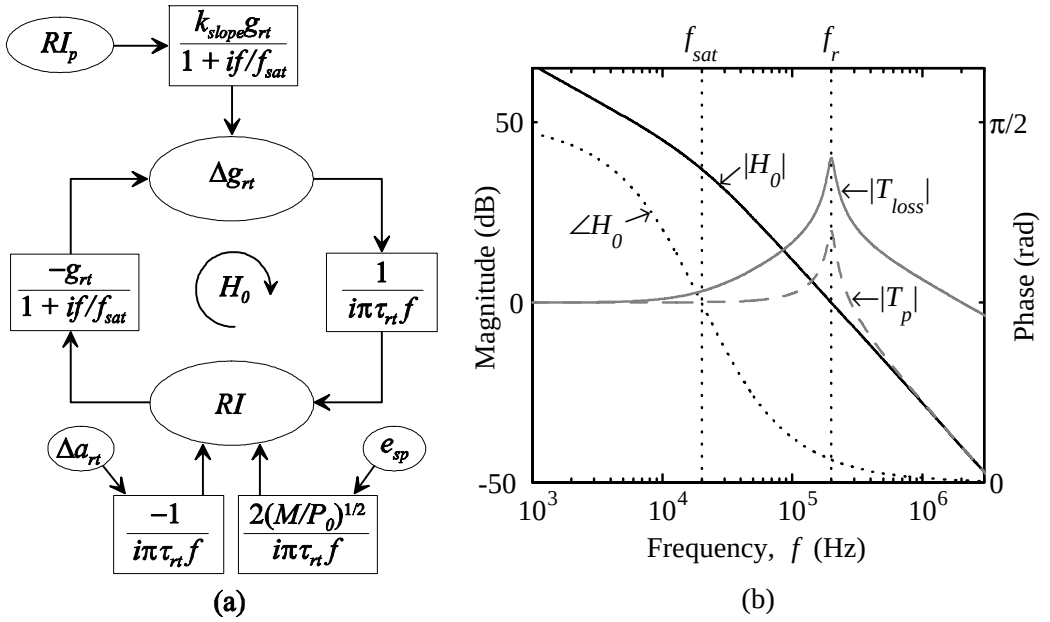

Figure 3.1. (a): Signal flow diagram illustrating the rate equations (3.6) in the frequency domain. (b): Phase and magnitude plots of the rondtrip transfer function $H_0(f)$ defined in (3.9); and arbitrarily scaled magnitude plots of the transfer functions T_p and $T_{loss} \propto T_{sp}\,(f)$ defined in (3.11). Parameters: $f_{sat} = 20$ kHz and $f_r = 200$ kHz.

The magnitudes of $T_p\,(f)$ and $T_{loss}\,(f) \propto T_{sp}\,(f)$ are illustrated Fig. 3.1 (b) with arbitrary scale factors. We see that the ratio between $T_{loss}\,(f)$ and $T_p\,(f)$ increases by 20 dB per decade for $f > f_{sat}$. Theoretical results recently published in [9] (for Er-doped lasers without ion clustering) are in qualitative agreement with Fig. 3.1 (b)[2].

The strong resonance in the transfer functions near $f = f_r$ is called the relaxation oscillation resonance. The strength of this resonance can be expressed by quality-factor Q_r, defined as the ratio of f_r to the 3-dB peak bandwidth of the transfer functions. For Er-doped fiber DFB lasers we will usually have $Q_r \gg 1$ (typically $Q_r > 8$), in which case the approximation $Q_r \approx [\angle H_0(f_r)]^{-1}$ is valid. Here, $\angle H_0(f_r)$ (expressed in radians) is the stability phase margin of H_0. From (3.9) and (3.10) we obtain

$$Q_r \approx f_r/f_{sat} = \sqrt{g_{rt}/(\pi\tau_{rt}f_{sat})}. \qquad (Q_r \gg 1) \tag{3.12}$$

[2]The dB-scales in different figures in [9] are not consistent. Apparently the scales in the first two figures should be multiplied by a factor of two.

By combining (3.12) and (3.7) we find that the laser stability can be expected to improve with increasing pump power P_p, increasing output power P_o, and decreasing laser mirror transmissivity M.

Saturable absorber states, which are believed to originate from clustering of Er^{3+} ions in highly Er doped fibers [10], or from UV-induced life-time quenching of the Er^{3+} ions [11] (discussed in Chap. 5), will contribute with a second feedback path to the RI that acts in parallel with the path shown in Fig. 3.1. The saturable absorber losses decrease with increasing laser intensity. The resulting modified roundtrip transfer function (3.9) can be written as:

$$H_0(f) = \frac{-f_r^2 f_{sat}^{-1}}{if(1+if/f_{sat})} + \frac{k_{s.abs}}{i\pi\tau_{rt}f}\,, \tag{3.13}$$

where $k_{s.abs} = \delta a_{rt}/\delta RI$ is a measure of the saturable absorber strength. The last term in (3.13) pulls the phase margin $\angle H_0(f_r)$ down by approximately $k_{s.abs}/(\pi\tau_{rt}f_r) \simeq k_{s.abs}\sqrt{g_{rt}/(\pi\tau_{rt}f_{sat})}$, and the stability of the laser is thus degraded by the saturable absorber. Although highly simplified,[3] we believe that (3.13) can be used to model the effects of saturable absorbers near $f = f_r$. More comprehensive models, requiring a detailed knowledge of the saturable absorber behavior (which we lack for the lasers studied in this chapter), are presented in [9, 10, 12]. Stability degradation due to saturable absorbers has been verified by several authors, including [10, 12]. On the other side, theoretical results in [9] indicate an improvement in stability (reduced Q_r) with increasing clustering fraction. There is no discussion in [9] of the reason for this unexpected result.

External feedback with time-delays that correspond to a significant phase shift at the relaxation oscillation frequency may also pull on the phase margin and cause degraded stability. Effects of external optical feedback and UV-induced saturable absorbers on laser stability will be discussed further in Chapters 4 and 5.

If the losses are dominated by the mirror transmissivities, and if both mirror transmissivities are equal to M (symmetric output), we will have $M = a_{rt} = g_{rt}$. For a discrete π phase-shifted DFB laser of length L we then have $M = 4\exp(-\kappa L)$, where κ is the index coupling parameter. Typical values for fiber DFB lasers may range from $M = 5\times10^{-6}$ to 5×10^{-3}.

The cavity roundtrip-time can be expressed as $\tau_{rt} = 2nL_c/c$, where L_c is the effective cavity length. For the π phase-shifted DFB laser it can be shown that $L_c \cong 1/\kappa$ (c.f. Chap. 1). If a distributed grating phase-shift is used, a length in the order of the extension of the phase-shift region should be added to the

[3] $k_{s.abs}$ will depend on the intracavity power P_o/M, and is expected to increase with P_o/M at low power levels. We expect $k_{s.abs}$ to saturate at high intracavity power levels, as the saturable absorber saturates. A frequency dependence of $k_{s.abs}$ is also expected for high frequencies f.

above value. Typical values for L_c may range from 3 to 15 mm, corresponding to roundtrip delays of $\tau_{rt} = 30 - 150$ ps.

3.2.4 Interactions with the Laser Frequency

In the following we discuss mechanisms related to the gain medium and the cavity loss dispersion that cause coupling or correlation between the intensity and frequency fluctuations in the laser.

Gain Medium Mechanisms

In semiconductor lasers, the linewidth enhancement factor α_g of the gain medium is known to play a dominating role in determining ν_{rms}. α_g relates refractive index changes to changes in the active gain in the cavity, and is defined by:

$$\alpha_g = \frac{dn'}{dn''} \tag{3.14}$$

where dn' and dn'' are changes in the complex refractive index $n'+in''$. The real and imaginary parts of the refractive index are related through the Kramers-Kronig relation.[4] Typical values for semiconductor lasers are $\alpha_g \sim 3 - 7$ [7]. α_g has been mentioned as a parameter of significance for longitudinal mode instabilities in semiconductor DFB lasers. We do not expect this to be the case for fiber DFB lasers, because the roundtrip gain magnitudes are generally orders of magnitude smaller than in semiconductor lasers. This means that the roundtrip phase-shift changes related via α_g to gain saturation will be small. There are still at least two reasons why the linewidth enhancement factor is of importance for fiber DFB lasers. First, the stability of the lasers in the presence of external reflection degrades with increasing α_g, as will be shown further down in this sub-section. Especially, the value of α_g at the relaxation oscillation frequency is of importance, as will become apparent in Chaps. 4 and 5. Second, the contribution from spontaneous emissions to the laser frequency noise ν_{rms} is proportional to α_g, as shown in Sec. 3.2.5.

Measured values of α_g in fiber lasers have to our knowledge not been reported in the literature. Simulation results for a saturated Er-doped amplifier reported by Alameh *et.al.* in [13] (based on theory published by Desurvire [14]) show the real and imaginary parts of the complex susceptibility for a few values of the saturating signal power P_s. Their results indicate that α_g increases when

[4] All physical (causal and stable) impulse responses must obey the Kramers-Kronig relations. However, both Desurvire [14] and Alameh *et.al.* [13] point out that the Kramers-Kronig relations are not valid for the complex susceptibility function they use to model saturation in Er^{3+}-doped amplifiers. This because the susceptibility function has poles in the right half of the complex s-plane, implying instability on time-scales longer than τ_{sat}. This must be due to approximations implicit in the model, as it cannot be true for the physical system.

the saturating signal power P_s or wavelength λ_s are increased. Their results indicate that α_g is roughly proportional to P_s for signal to saturation power ratios in the range $P_s/P_{sat} = 10 - 20$. (See Chapter 6 for a definition of P_{sat}.) For $P_s/P_{sat} \approx 20$ we estimate from [13] that α_g goes through zero around $\lambda_s = 1540$ nm, increasing to $\alpha_g \sim 2.3$ at 1550 nm and $\alpha_g \sim 4.4$ at 1560 nm. The main contribution to the calculated refractive index change seems to come from spectral hole-burning of the gain population for wavelengths close to λ_s. It should be noted that the results in [13] are derived for steady-state saturating conditions, i.e. for $f \ll f_{sat}$. Typical values for f_{sat} inside fiber DFB lasers are expected to be in the range from $5 - 160$ kHz (depending mostly on the grating strength). It is unclear to which degree the theory in [13] leads to representative values for α_g for $f > f_{sat}$. More comprehensive studies of the factors influencing on α_g could be useful, including studies of how α_g depends on f, P_s, P_{sat}, λ_s, pump wavelength, fiber composition (codopants), ion clustering, UV-induced lifetime quenching, etc.

α_g can be expressed in terms of the ratio between changes in the laser frequency ν and the cavity roundtrip gain $\Delta g_{rt} = \frac{1}{2}\tau_{rt} dRI/dt$, or alternatively in terms of the ratio between changes in the optical phase ϕ_s and the RI. From (3.14) we derive:

$$\alpha_g = 2\pi\tau_{rt}\frac{\partial\nu}{\partial g_{rt}} = \left\{\frac{2\,d\phi_s}{dRI}\right\}_{gain} \tag{3.15}$$

The subscript "*gain*" is used to indicate that only contributions to the differentials from the saturation of the gain medium is included. (3.15) indicates that we can estimate α_g from measurements of the correlation (or transfer function) between RI and ϕ_s ($= \Delta\nu/if$) provided that we can identify which fraction of the RI that originates from gain fluctuations. The direct input contributions to the RI from Δa_{rt} and e_{sp} in Fig. 3.1 (a) do not originate from the gain medium.

At the relaxation oscillation resonance frequency, the external input contributions to the RI will be amplified due to the feedback resonance by the quality factor Q_r, which is typically high in Er-doped fiber DFB laser ($Q_r \sim 8 - 50$). Therefore, the main contribution to RI in Fig. 3.1 (a) comes through the path from Δg_{rt}, and we can use the approximation $\Delta g_{rt} \approx i\pi\tau_{rt} f\, RI$. Inserting this approximation into (3.15) (with $\partial\nu/\partial g_{rt} = \Delta\nu/\Delta g_{rt}$) we obtain:

$$\alpha_g \simeq \frac{2\Delta\nu}{if\,RI} \quad \text{(relaxation oscillations, } Q_r \gg 1), \tag{3.16}$$

where $\Delta\nu$ is the measured frequency shift.

More general formulas that can be used to express α_g in terms of the normalized correlation $\langle\Delta\nu^* RI\rangle/(\nu_{rms} RIN)$ between $\Delta\nu$ and the RI outside the

relaxation oscillation resonance are deduced in [7]. However, due to the thermal effects discussed below, we expect $\langle \Delta\nu^* RI \rangle / (\nu_{rms} RIN)$ to depend heavily on which of the sources in Fig. 3.1 (a) that cause the RI. Care should therefore be taken when interpreting the results of applying these formulas to Er-doped fiber lasers.

Heating Mechanisms

Self heating from non-radiative losses of laser and pump energy will also contribute to a correlation between the RI and $\Delta\nu$. The relaxation of gain ions from the pump absorption level to the upper laser level is one source of self heating. Non-radiative losses at the pump and laser wavelengths are other possible sources. The self heating can be characterized by the ratio:

$$r_{th} = \frac{\Delta\nu_{th}}{RI}, \tag{3.17}$$

where $\Delta\nu_{th} = \frac{\delta n}{n\delta T}\Delta T$ is the thermally induced frequency shift, $\frac{\delta n}{n\delta T}$ is the effective thermal sensitivity (including effects of thermal stress and strain) of the refractive index n, and ΔT is the temperature change. For $f \ll f_r$, the fluctuations ΔP_{th} in the thermal power P_{th} produced in the core is expected to be proportional to the RI. At low frequencies f where the fiber core is in thermal equilibrium with the cladding and surroundings, we therefore expect a frequency independent proportional relation $\Delta\nu_{th} \propto \Delta T \propto -\Delta P_{th} \propto -RI$, and thus a frequency independent negative value for r_{th}.[5] Note, however, that the proportionality constant relating ΔP_{th} to RI depends on which of the self heating sources that dominate. This again depends on which of the input noise sources RI_p, Δa_{rt} and e_{sp} that dominates the laser noise.

For $f \gtrsim f_r$ a frequency independent proportionality between the RI and ΔP_{th} can no longer be assumed, partly because $T_p(f)$ becomes frequency dependent. It is also necessary to take Δg_{rt} into account as a significant source of fluctuations in the pump absorption rate. The thermal contribution $\alpha_{g,th}$ to α_g near $f = f_r$ can be expressed by combining (3.16) and (3.17) as:

$$\alpha_{g,th} = 2\pi\tau_{rt} \left\{ \frac{d\nu}{dg_{rt}} \right\}_{thermal} \simeq \frac{2r_{th}}{if} \quad \text{(relaxation oscillations, } Q_r \gg 1\text{)}. \tag{3.18}$$

Loss Dispersion Mechanisms

Fluctuations $\Delta\nu$ in the cavity resonance frequency due to refractive index perturbations that modify the effective cavity roundtrip phase-shift can in principle lead to laser intensity noise through the optical frequency dependence of

[5] The upper frequency limit for the condition of thermal equilibrium to be true depends on the nature of the heat sink. For an ideal heat sink with constant temperature at the fiber surface, we see from Fig. 3.6 that the upper frequency limit is about 100 Hz.

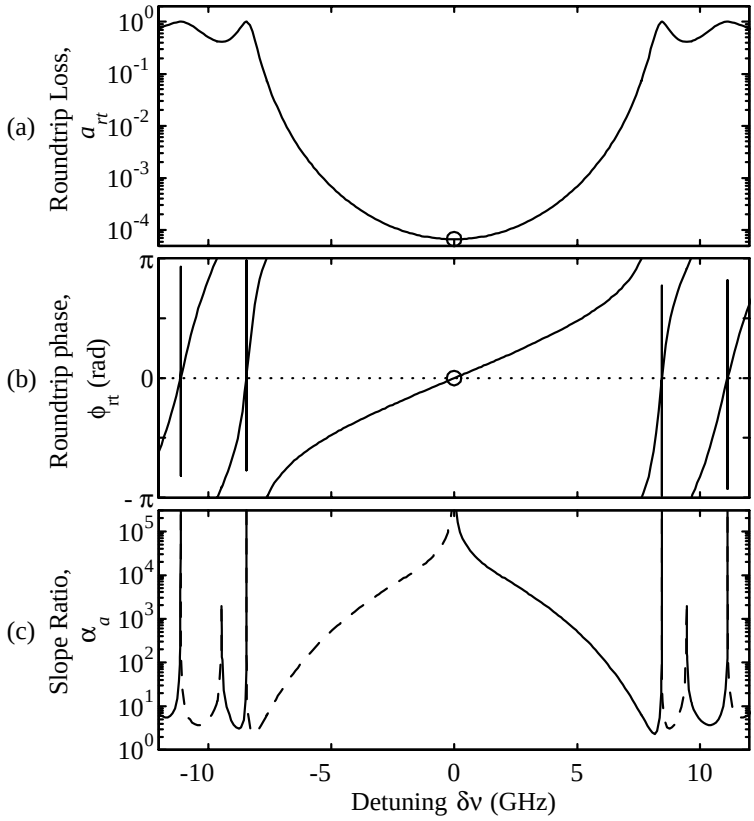

Figure 3.2. Roundtrip loss a_{rt} (a) and phase ϕ_{rt} (b) versus detuning $\delta\nu$ for an ideal 50 mm DFB laser with $\kappa L = 11$. Circles (○) indicate the laser operation point. (c) Ratio α_a (3.19) between the slopes of ϕ_{rt} and a_{rt}. Dashed lines indicate negative values.

the grating mirror transmissivities. Fig. 3.2 (a) shows the cavity roundtrip loss a_{rt} versus frequency detuning $\delta\nu$ for an ideal π phase-shifted fiber DFB laser of length $L = 50$ mm with a normalized index coupling coefficient of $\kappa L = 11$. The laser operation point at $\delta\nu = 0$ is indicated by a circle. We see that the loss is frequency independent at this point. Frequency perturbations will therefore not to the first order cause intensity noise in an ideally phase-shifted DFB laser.

Fig. 3.2 (b) shows the roundtrip phase $\phi_{rt}(\delta\nu)$ of the same laser. (The steep phase transitions at ± 8.4 and ± 11.1 GHz are due to higher order resonances of the DFB grating.) A change $\Delta\phi_{rt}$ in the effective grating phase-shift will cause ϕ_{rt} to move vertically in the figure by $\Delta\phi_{rt}$. The laser resonance frequency must still be at the zero-crossing $\phi_{rt}(\delta\nu) = 0$, and will thus move by $\Delta\nu = -\Delta\phi_{rt}/(d\phi_{rt}/d\delta\nu) = -\Delta\phi_{rt}/(2\pi\tau_{rt})$, since $d\phi_{rt}/d\delta\nu = \tau_{rt}$.

Inspired by (3.15) we define the "loss dispersion linewidth broadening factor" as:

$$\alpha_a = 2\pi\tau_{rt}\frac{\partial\nu}{\partial a_{rt}} = 2\pi\frac{d\phi_{rt}}{d\nu}\frac{\partial\nu}{\partial a_{rt}} = \left\{\frac{d\phi_{rt}/d\nu}{da_{rt}/d\nu}\right\}_{loss} \tag{3.19}$$

α_a is plotted for the ideal DFB laser in Fig. 3.2 (c).

In the presence of a small gain perturbation $\Delta\gamma$ (either due to loss, spontaneous emission or pump fluctuations), the interaction between α_a and α_g can be expressed by an effective linewidth enhancement factor $\alpha_{eff} = 2\pi\tau_{rt}\Delta\nu/\Delta\gamma$. At low frequencies $f \ll f_r$ we may assume $g_{rt} - a_{rt} = 0$, implying:

$$\Delta\nu\left\{\frac{\partial\nu}{\partial g_{rt}}\right\}^{-1} - \Delta\nu\left\{\frac{\partial\nu}{\partial a_{rt}}\right\}^{-1} + \Delta\gamma = 0.$$

Substituting $\partial\nu/\partial g_{rt}$ and $\partial\nu/\partial a_{rt}$ from (3.19) and (3.15) we obtain:

$$\alpha_{eff} = 2\pi\tau_{rt}\frac{\Delta\nu}{\Delta\gamma} = \frac{1}{\alpha_g^{-1} - \alpha_a^{-1}}. \tag{3.20}$$

The interaction between α_a and α_g will also affect the laser response to frequency perturbations. Assume that the laser is perturbed so that the frequency would change by $\Delta\nu_0$ for $\alpha_g = 0$ (for instance due to a perturbation of the cold cavity resonance frequency, or to spontaneous emission). The frequency change when the effect of α_g is taken into account is denoted $\Delta\nu$. Again assuming $g_{rt} - a_{rt} = 0$ we have:

$$(\Delta\nu - \Delta\nu_0)\left\{\frac{\partial\nu}{\partial g_{rt}}\right\}^{-1} - \Delta\nu\left\{\frac{\partial\nu}{\partial a_{rt}}\right\}^{-1} = 0.$$

implying:

$$\frac{\Delta\nu}{\Delta\nu_0} = \frac{\alpha_g^{-1}}{\alpha_g^{-1} - \alpha_a^{-1}} = \frac{\alpha_{eff}}{\alpha_g}. \tag{3.21}$$

The initial frequency perturbation $\Delta\nu_0$ is magnified by the ratio α_{eff}/α_g.

We see from (3.20) and (3.21) that α_a must be smaller than or comparable to α_g in magnitude in order to affect the laser noise significantly. From Fig. 3.2 (c) we see that this will not be the case for the ideal fiber DFB laser if it operates in the fundamental mode and within the grating stop band limits $|\delta\nu| < 7$ GHz. The figure indicates, however, that α_a may be of importance for lasers operating in higher order modes.

External reflections will cause ripple in the curves in Fig. 3.2 (a) and (b), and they will therefore contribute to α_a. If the external amplitude reflectivity

is r_e with a delay τ_e that satisfies $\tau_{rt} \ll \tau_e < \tau_{coh}$, the frequency dependence of the roundtrip loss and phase can be approximated by:

$$\begin{aligned} \Delta a_{rt} &\simeq M r_e \cos 2\pi\nu\tau_e \\ \Delta\phi_{rt} &\simeq 2\pi\Delta\nu\tau_{rt} + M r_e \sin 2\pi\nu\tau_e. \end{aligned} \tag{3.22}$$

Here M is the mirror transmissivity to the laser port that is connected to the external cavity. α_a follows from (3.19) and (3.22) as:

$$\alpha_a = -\frac{1 + M r_e \tau_e/\tau_{rt} \cos 2\pi\nu\tau_e}{M r_e \tau_e/\tau_{rt} \sin 2\pi\nu\tau_e} \quad \text{(External reflection)}. \tag{3.23}$$

For reflections satisfying $M r_e \tau_e/\tau_{rt} \ll 1$ we have that $|\alpha_a^{-1}| \ll 1$ for all optical frequencies ν, implying that the back reflection is not of significance for the value of α_{eff}.

From (3.20) we see that $\alpha_{eff} \to \infty$ if $\alpha_a^{-1} \to \alpha_g^{-1}$. The maxima in $|\alpha_a^{-1}|$ with respect to ν occurs for $\cos 2\pi\nu\tau_e = -M r_e \tau_e/\tau_{rt}$. The condition $\alpha_a^{-1} = \alpha_g^{-1}$ will occur at every second of these minima if:

$$M r_e \tau_e/\tau_{rt} = \left(1 + \alpha_g^2\right)^{-1/2} \quad \text{(critical external reflection)}. \tag{3.24}$$

At this and higher back-reflection levels $\alpha_{eff}(\nu)$ will go through singularities for certain values of ν, corresponding to mode-hopping between external cavity modes. Equation (3.24) is consistent with the external mode-hopping criterion $C \geq 1$ used in Chap. 5. The effect of external back reflections on the stability and the effective linewidth enhancement factor of semiconductor lasers is reviewed by Petermann in [15].

3.2.5 Schawlow-Townes Noise Limit

In Sec. 3.2.2 we mentioned that the spontaneous emission seeding of the laser operation causes a direct contribution to ϕ_{rms} with magnitude $M^{1/2} e_{sp}/(\pi\tau_{rt} f|A|)$. It can be shown that this magnitude must be multiplied by $(1+\alpha_{eff}^2)^{1/2}$ to incorporate the phase noise from the spontaneous emission induced fluctuations in Δg_{rt} at $f \ll f_r$. Using $\nu_{rms} = f\phi_{rms}$ we obtain the frequency noise due to spontaneous emission seeding of the laser operation as:

$$\nu_{rms} = \sqrt{1 + \alpha_{eff}^2}\, \frac{e_{sp}\sqrt{M}}{\pi\tau_{rt}|A|} \quad (f \ll f_r, \text{ spontaneous emission}). \tag{3.25}$$

From (3.5) and (3.25) we obtain

$$\Delta\nu_{3dB} = \left(1 + \alpha_{eff}^2\right) \frac{e_{sp}^2\, M}{\pi\tau_{rt}^2 P_o} \quad (f \ll f_r, \text{ spontaneous emission}), \tag{3.26}$$

where $P_o = |A|^2$ is the laser output power.

The lowest possible value for e_{sp}^2 equals $2h\nu\, a_{rt}$, and is obtainable if the gain medium has the lowest possible doping concentration that will allow for threshold gain at full inversion. By inserting $e_{sp}^2 \geqslant 2h\nu\, a_{rt}$ into 3.26 we obtain:

$$\Delta\nu_{3dB} \geqslant \left(1 + \alpha_{eff}^2\right) \frac{2h\nu\, a_{rt}\, M}{\pi \tau_{rt}^2 P_o} \qquad \text{(spontaneous emission)} \tag{3.27}$$

(3.27) is known as the Schawlow-Townes noise limit (originally derived for $\alpha_{eff} = 0$), after A. L. Schawlow and C. H. Townes who were central in the early work on laser science from the late 1950's and onwards.

Typical fiber DFB lasers have values for the ratio $a_{rt}M/\tau_{rt}^2$ that are many orders of magnitude smaller than what is usually obtainable with semiconductor laser. This implies that smaller linewidths are obtainable with fiber DFB lasers. External cavity lasers, ring lasers, Fabry-Perot fiber lasers, or large bulk lasers may have much higher effective values for τ_{rt}, but the task of maintaining stable single longitudinal mode operation generally becomes more difficult as τ_{rt} increases. Frequency modulation noise densities which are believed to be dominated by spontaneous emission noise above $f \approx 3$ kHz have been reported for distributed back reflection (DBR) fiber Bragg grating lasers with relatively high cavity losses ($a_{rt}, M \sim 0.05$) [16].

With parameter values obtainable for fiber DFB lasers of $a_{rt} = M = 10^{-5}$, $\tau_{rt} = 50$ ps, $P_o = 250$ μW, $\alpha_{eff} = 3$, and $\nu = 194$ THz ($\lambda_s = 1550$ nm) we obtain $\Delta\nu_{3dB} \geqslant 0.13$ mHz. From slope efficiency considerations, and to allow for 1480-nm intraband pumping which allows for a maximum of about 75 % inversion, doping concentrations that are considerably higher than the theoretical requirement at full inversion may be desirable. In practical fiber DFB lasers, e_{sp}^2 may therefore be from 10 to 1000 times larger than the theoretical minimum of $2h\nu\, a_{rt}$ assumed in (3.27). The spontaneous emission induced frequency noise (3.26) of typical fiber DFB lasers is still believed to be well below other noise contributions, such as the fundamental thermal noise in the fiber index discussed in Subsec. 3.3.

3.2.6 Shot Noise

The shot noise, which is due to the quantization of the light into photons with energy $h\nu$, puts a lower limit to the detected RIN given by:

$$RIN = \sqrt{\frac{2h\nu}{P_o}} \qquad \text{(Shot noise).} \tag{3.28}$$

A common method for optical frequency interrogation is by use of Mach-Zehnder or Michelson interferometers. When operated in quadrature with balanced detection, such interferometers can achieve a noise equivalent frequency

shift $NE\nu$ due to the shot noise at the detectors of:

$$NE\nu = \frac{RIN \times f}{2\,|\sin(\pi\tau_i f)|} = \sqrt{\frac{h\nu}{2P_o}}\frac{f}{|\sin(\pi\tau_i f)|}\,, \qquad \text{(Interferometer shot noise)} \tag{3.29}$$

where τ_i is the interferometer delay and RIN is expressed by (3.28). For low frequencies $f \ll \tau_i^{-1}$ we have $NE\nu = RIN/(2\pi\tau_i)$. Thus, an interferometer with $\tau_i = 0.5$ μs (about 100 m single pass optical delay fiber) and a detected power of P_o of 1 μW will have a low-frequency $NE\nu$ of 160 mHz/$\sqrt{\text{Hz}}$.

$NE\nu$ according to (3.29) can be minimized for a given frequency f by choosing an interferometer delay τ_i that is an odd multiple of $(2f)^{-1}$. This produces an expression for what we believe is the fundamental shot noise limit of the optical frequency detection:[6]

$$NE\nu = \sqrt{\frac{h\nu}{2P_o}}f \qquad \text{(Shot noise)} \tag{3.30}$$

Note that $NE\nu$ according to (3.30) is proportional to f. It can be shown that the $NE\nu$ predicted by (3.30) can be obtained simultaneously for all frequencies f by heterodyne detection systems employing electrical beat-frequency interrogation of the optical detector output.

If an optical amplifier is used to increase the input power to the interrogation system, the lower limit for $NE\nu$ increases by at least 3 dB (depending on the amplifier noise figure) compared to the level predicted by (3.30), due to mixing with the amplified spontaneous emission.

3.3 Temperature Fluctuations

An important source of laser frequency noise is refractive-index fluctuations in the cavity due to temperature fluctuations. The resonance frequency of fiber lasers at 1550 nm has a temperature sensitivity of about -1 GHz/K (8 pm/K) [4], as verified in Chap. 8. There are three main sources of temperature fluctuations in the cavity: Ambient temperature fluctuations, self heating, and fundamental temperature noise due to random diffusion of thermal energy across the mode field boundary. Self heating will be treated in Sec. 3.5.

3.3.1 Ambient Temperature

The response of the laser to ambient temperature fluctuations is expected to decrease rapidly at frequencies above ~ 1 kHz if the bare fiber is only in contact

[6] An alternative way of arriving at (3.30) is by assuming that the rms contributions from quantization to the relative amplitude $RIN/2$ and phase ϕ_{rms} noise signals are equal. Inserting (3.28) into $NE\nu = \phi_{rms} f = 2RINf$ produces the result in (3.30).

with air. This is due to the limited thermal conductivity through the air-fiber interface and from the fiber surface to the core, as illustrated by Fig. 1 in [17]. If the fiber is surrounded by a material with higher thermal diffusivity than air the low-pass cut-off frequency of the response into the fiber may increase somewhat. On the other hand, a good heat sink will often act as an effective thermal low-pass filter on its own.

3.3.2 Fundamental Thermal Noise

If temperature is defined as the *expectation value* $\langle T \rangle = \langle E_{th}/C \rangle$ of the stored thermal energy E_{th} per unit heat capacity C, then the temperature of an object in thermal equilibrium with its surroundings must be independent of time. The effective refractive index of the fiber is, however, determined by the *instantaneous* temperature $T = E_{th}/C$ averaged over the mode power area $\pi MFD^2/8$ of the fiber. MFD is the mode-field diameter where the mode power density has dropped to e^{-2} of its maximum. Even for a fiber in perfect thermal equilibrium with its surroundings, there exists a thermal noise floor for the variance of the instant temperature fluctuation $\Delta T = T - \langle T \rangle$. This noise is caused by random diffusion of thermal energy in and out of the mode power area. Kingston [18] shows that this variance integrated over all frequencies f is given by:

$$\int_0^\infty \Delta T^2(f) df = \frac{k_b T^2}{C}\,, \tag{3.31}$$

where $k_b = 13.81 \times 10^{-24}$ J/K is Boltzmanns constant. For our case of a fiber laser, C is the heat capacity of the effective mode power volume, given by:

$$C = \frac{L_c \pi MFD^2}{8} C_V\,, \tag{3.32}$$

where $C_V = 1.67 \times 10^6$ J/(m^{3}K) is the specific heat capacity of silica.

The spectral power distribution $\Delta T^2(f)$ of this noise can be found by modelling the fiber as a collection of small heat capacities that are connected to their neighboring elements through thermal conductors. In analogy with the theory for thermal noise in electrical conductors, the random diffusion of heat can be represented as a heat (or "current") source Q_i in parallel with each conductor G_i with a white noise power spectral density $\langle Q_i \rangle = 4k_b T^2 G_i$. Due to the circular symmetry of the fiber, heat conduction and generation in the azimuthal direction will not contribute to ΔT. Heat conduction and generation in the longitudinal direction can also be neglected for $f \gg D/L_c^2$ where D is the effective thermal diffusivity of the combined fiber and surrounding materials. For a fiber with an infinite silica cladding, D/L_c^2 will be in the

order of $3 - 40$ mHz for typical fiber DFB laser cavity lengths. A numerical investigation into the shape of $\Delta T^2(f)$ and how it depends on fiber diameters, coating parameters, and heat sinking materials should be possible with typical available computer resources.

$\Delta T^2(f)$ is hard to compute analytically for the fiber geometry. An expression for the case of insulating border conditions at the fiber surface has been published by K. H. Wanser in [19]. The laser frequency noise magnitude derived from his formula may be expressed as

$$\nu_{rms}^2 = \left(\frac{\delta n}{n \delta T} + \frac{\delta \varepsilon}{\delta T} \right)^2 \nu_0^2 \, \Delta T^2(f) \; , \tag{3.33}$$

where

$$\Delta T^2(f) = \frac{k_b T^2}{2\pi k_c L_c} \times \ln \left\{ \frac{\left[\left(\frac{2}{\pi MFD} \right)^2 + \left(\frac{f}{c/n} \right)^2 \right]^2 + \left(\frac{f}{2\pi D} \right)^2}{\left[\left(\frac{2.405}{\pi d} \right)^2 + \left(\frac{f}{c/n} \right)^2 \right]^2 + \left(\frac{f}{2\pi D} \right)^2} \right\} . \tag{3.34}$$

Here, D the thermal diffusivity and $k_c = C_V D$ is the thermal conductivity of silica. $\delta\varepsilon/\delta T$ is the thermal expansion coefficient (ε = strain),[7] $n \approx 1.465$ is the refractive index, $c = 3 \times 10^8$ m/s is the speed of light in vacuum, d is the fiber diameter, and MFD is the modefield diameter. Typically, $d = 125\,\mu$m or $80\,\mu$m, while $MFD \approx 9.4$ μm for standard fiber, and 5.8 μm for high NA Er-doped fiber.

The derivation of (3.34) has not been published. Wanser takes thermal and optical material parameters for silica fiber from [20]: $k_c \approx 1.37$ W/(m K); $D \approx 0.82 \times 10^{-6}$ m^2/s; $(\delta n/(n\delta T) \approx 9.2 \times 10^{-6}$ K^{-1}; and $\delta\varepsilon/\delta T = 0.4 \times 10^{-6}$ K^{-1}. However, the temperature sensitivity of silica fibers generally accepted elsewhere in literature (and also verified in Chap. 8) $(\delta n/(n\delta T) + \delta\varepsilon/\delta T) \approx 5.2 \times 10^{-6}$ K^{-1} [4, 17] is only about one half of the value used in [19, 20]. Experimental results reported for the frequency range $f \sim 1 - 100$ kHz have been compared in [5, 21, 22, 23] with Wansers formula, using the material parameters as in [19, 20]. These experiments show noise floors which are similar in shape, and $1 - 3$ dB *above* the theoretical predictions.

Numerical calculation of the integral on the left-hand side of eq. (3.31) with $\Delta T^2(f)$ inserted from (3.34) produces a result that is a factor of two smaller

[7] It can be argued that the fiber expansion will not be proportional to only the core temperature fluctuations ΔT for frequencies well above 1 kHz, because the temperature will not be correlated across the whole fiber cross-section at these frequencies. Consequently, we believe that the term $\delta\varepsilon/\delta T$ should be omitted from (3.33) at higher frequencies.

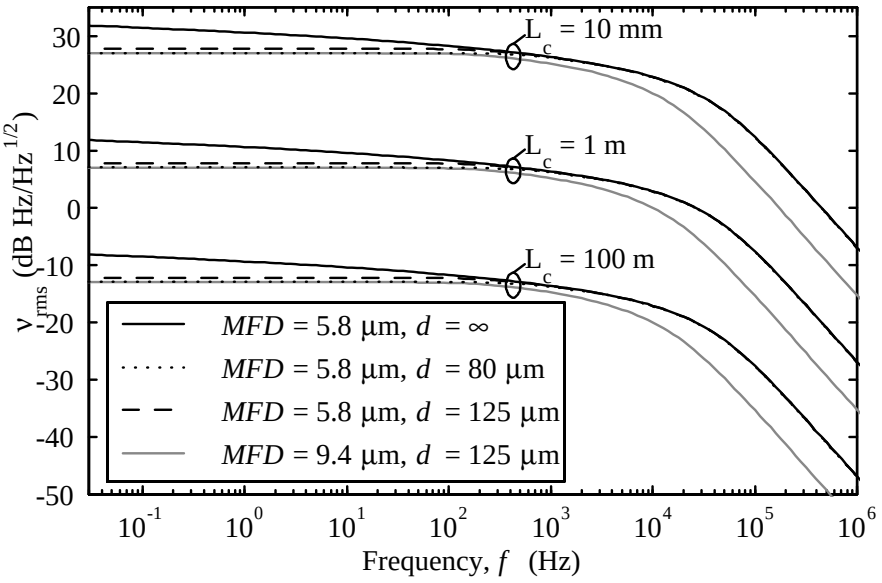

Figure 3.3. Fundamental thermal noise of the resonance frequency of fiber-optic cavities with length $L_c = 0.01$, 1 and 100 m, according to (3.33, 3.34) with 6 dB added for conformity with reported experiments.

than the right-hand side of eq. (3.31). This result is independent on the choice of material parameters. Since the shape of $\Delta T^2(f)$ predicted by (3.34) has been verified experimentally for $f > 1$ kHz, we believe that the discrepancy with (3.31) must either be due to a scaling error, or to an error in the frequency dependence of (3.34) (the logarithmic term) for $f < 1$ kHz.

In lack of better expressions, we will use (3.33, 3.34) in the following to illustrate the expected thermal frequency noise floor, using $(\delta n/(n\delta T) + \delta\varepsilon/\delta T) \approx 5.2 \times 10^{-6}$ K^{-1} and with 6 dB added for conformity with the previously reported experiments. Fig. 3.3 shows this noise floor for various values of L_c, d, and MFD. For $f > 100$ Hz the noise decreases by 20 dB/decade, while a strong dependence on MFD is observed at high frequencies, approaching $\nu_{rms} \propto (MFD)^{-2}$ for $f > 100$ kHz. This dependence on MFD is in agreement with (3.31, 3.32). For $f < 100$ Hz ν_{rms} increases with increasing fiber diameter. The results below 1 kHz should be used with care, however, since experimental evidence are not available for this regime.

According to [20], noise contributions due to direct interaction with thermal phonons will dominate over the temperature noise for $f \gtrsim 1$ MHz, increasing by 20 dB/decade towards a maximum around 500 MHz. The phonon contributions are not included in Fig. 3.3.

3.4 Acoustical Noise

The sensitivity of the laser to acoustical noise depends much on how it is mounted. If the laser is fixed in each end and strained, it will be sensitive to mechanical vibrations in the distance between the fixing points. The strain sensitivity of the laser is about 150 Hz/pε. If the laser is mounted with some slack, the problems with strain sensitivity should be reduced. However, high frequency vibrations in the supporting structure may still couple to compressional and flexural waves in the laser fiber. The sensitivity of a fiber with slack to mechanical perturbations has not yet to our knowledge been studied in the literature.

The sensitivity of the laser to pressure waves may also play a role. If the laser is submerged into a liquid, like water or oil, the sensitivity is expected to be $\sim$ 870 Hz/Pa if the fiber is axially constrained, and ~ -520 Hz/Pa if the fiber is free to expand [21]. At low frequencies (typically $f < 50$ kHz), the free expansion sensitivity should be used if the fiber is mounted with slack. At higher frequencies the treatment becomes more complex, as the acoustical wavelength for compression waves in the fiber becomes comparable to the fiber length.

The sensitivity of the fiber DFB laser to acoustical vibrations in air has been studied both theoretically and experimentally in [17], and was found to range from about 600 kHz/Pa at $f = 100$ Hz to about 2 kHz/Pa at $f = 7$ kHz. This implies that an acoustical noise amplitude of 20 dBA (200 μPa) at $f = 100$ Hz will cause a laser frequency noise amplitude of $\nu_{rms} = 120$ Hz. The acoustical sensitivity at low frequencies is dominated by adiabatic temperature changes induced by the acoustic compression of the air. The high sensitivity to acoustical noise at low frequencies can therefore easily be avoided by immersing the fiber into a liquid, which will not compress and heat significantly in response to acoustic waves.

3.5 Pump Fluctuations

In Sec. 3.2.3 it was shown that fluctuations in the relative pump intensity RI_p will cause laser RIN through the transfer function $T_p(f)$ (3.11). If saturable absorbers are present, the pump will also modulate the saturable absorber losses at the laser wavelength, causing additional RIN contributions through $T_{loss}(f)$. The pump induced RIN will lead to frequency noise according to the frequency to intensity noise ratio r_{th} (3.17) at low frequencies $f \ll f_r$ and according to the linewidth enhancement factor α_g (3.16) at $f \approx f_r$.

Fig 3.4 shows a typical measured response of the optical frequency shift $\Delta\nu$ and the relative laser intensity RI to modulation of RI_p for a fiber DFB laser.

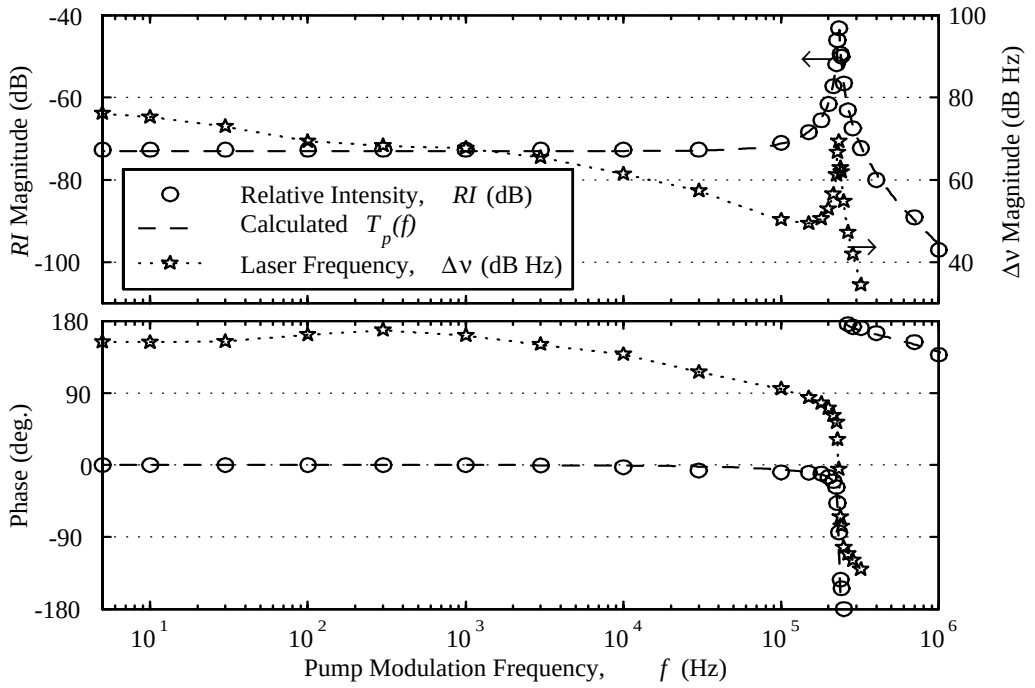

Figure 3.4. Response of the relative intensity RI and optical frequency $\Delta\nu$ of an Er-doped fiber DFB laser to pump modulation. The1480-nm pump power was modulated around its mean value of 60 mW with an rms amplitude of ~ 2.5 μW.

The pump power to the laser was modulated with an amplitude of about 2.5 μW rms by modulating the drive current to the pump diode, corresponding to a relative pump intensity modulation of $RI_p = -73.7$ dB.

The investigated laser was a sealed Er-doped fiber DFB laser (Ionas IFL01W1E-AD) operating at 1558 nm. The fiber laser was pumped with 60 mW at 1480 nm from a laser diode through a 1480/1550 nm wavelength division multiplexer (WDM). The output from the laser was about 170 μW copropagating with the pump, with a slope efficiency of ~ 3.3 μW/mW. The composition of the fiber laser heat sink is not known. The output from the 1550 nm branch of the WDM was passed through an isolator and split by a 10:90 fiber coupler.

The 90 % output from the 10:90 coupler was passed to a detector for monitoring of the RI. The 10 % output was passed to a Michelson interferometer with a dual pass path imbalance of 69 m ($\tau_i = 337$ ns). Balanced detection by subtracting the detected output power from one interferometer port from the output from the other port was used in order to minimize the sensitivity of the readout to laser RIN. In order to keep the interferometer in quadrature, the error signal generated at the balanced receiver output was fed back to a PZT optical phase modulator in one of the interferometer arms via a time-domain

integrator filter. By adding the high-frequency ($f \gtrsim 1.5$ kHz) error signal to the low-frequency PZT signal (using proper scale factors), $\Delta\nu$ could be monitored from DC and up to $f > 1$ MHz. The plotted responses are calibrated to remove effects of the frequency responses of pump driver and detector electronics, as well as interferometer responses and fiber transmission delays.

The dashed line in Fig. 3.4 shows the pump response $T_p(f)$ calculated from (3.11, 3.13) with the parameters $k_{slope} = 1.18$, $f_r = 238$ kHz, $f_{sat} = 52$ kHz, $k_{s.abs} = 1.4 \times 10^{-5}$, and $\tau_{rt} = 1 \times 10^{-10}$ s ($\Leftrightarrow L_c = 10$ mm). Good fits to the measured RI magnitude can also be obtained with other combinations of f_{sat} and $k_{s.abs}$. The fit to the phase of the RI response for $f > f_r$ does, however, indicate that the chosen values f_{sat} and $k_{s.abs}$ are reasonable.

As mentioned in the introduction to this section, any modulation of the saturable absorber losses by the pump power modulation is expected to give a contribution to the pump modulation response that is proportional to $T_{loss}(f)$. From Fig. 3.1 (b) we see that the shape of the $T_{loss}(f)$ differs significantly from that of $T_p(f)$ at frequencies $f > f_{sat}$. It is therefore not possible to obtain a good fit to the measurements in Fig. 3.4 with our model if pump induced loss modulation is assumed to play a significant role.

Fig. 3.5 shows an expanded view of the relaxation oscillation peak. The relaxation oscillation resonance Q-factor is found from the measurements to be $Q_r = 31$, which is relatively high. Typical values measured for other lasers range from $Q_r = 10$ and upwards.

The shot noise induced RIN for our laser according to (3.28) is -148 dB Hz$^{-1/2}$. To avoid that pump-induced RIN dominates over shot-noise we then find from Figs. 3.4 and 3.5 that the requirements are $RIN_p < -148.7$ dB Hz$^{-1/2}$ at low frequencies $f \ll f_r$, and $RIN_p < -179$ dB Hz$^{-1/2}$ at $f = f_r$. To operate below the thermal noise floor for ν_{rms} predicted by (3.33) with $L_c = 10$ mm, the requirements become $RIN_p < -115$ dB Hz$^{-1/2}$ at $f = 100$ Hz and $RIN_p < -137$ dB Hz$^{-1/2}$ at $f = f_r$.

The shot-noise limitation of the effective RIN_p experienced by the fiber laser comes from the quantization of the absorbed pump energy. The shot noise statistics of this absorption gives an effective noise magnitude [in analogy with (3.28)] of $RIN_p = (2h\nu_p/P_{p,abs})^{1/2}$, where $h\nu_p$ is the pump photon energy and $P_{p,abs}$ is the pump power absorbed within the laser cavity by active gain ions. A simple estimate for the pump absorption would be $P_{p,abs} = 1550/1480 \times 2P_o = 356$ μW, ignoring intracavity losses and assuming equal outputs from the two laser ends. The effective pump shot noise limitation then becomes $RIN_p = -151$ dB Hz$^{-1/2}$. This is 28 dB below the requirement for shot-noise limited RIN at $f = f_r$ stated in the last paragraph. Consequently, stabilization the pump laser intensity is not sufficient to avoid that the RIN raises at least 28 dB above the shot noise limit at $f = f_r$.

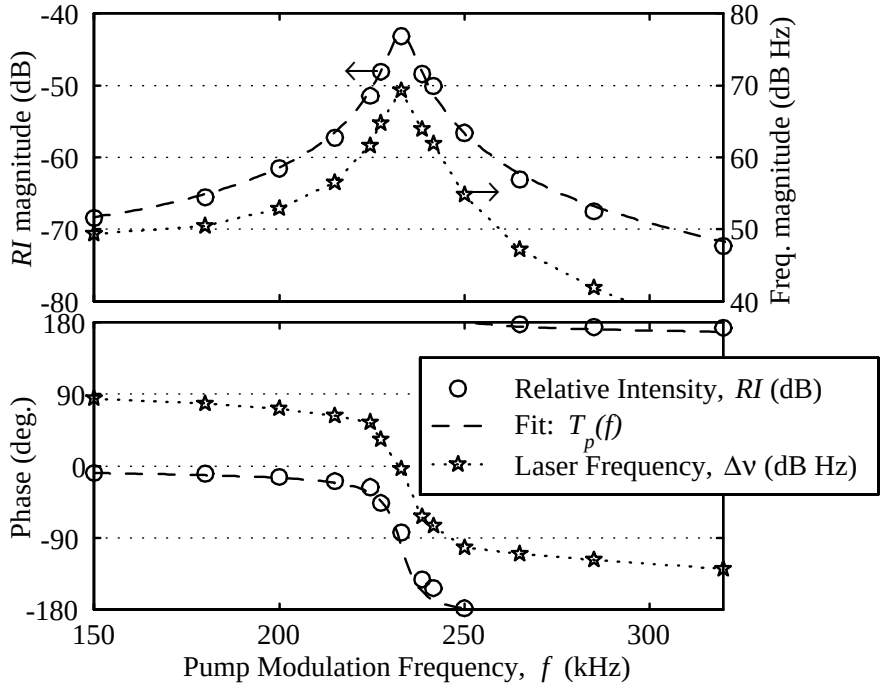

Figure 3.5. Expanded view of the relaxation oscillation peak in Fig. 3.4.

Fig. 3.6 shows the ratio $\Delta\nu/RI$ of the pump modulation responses. Circles illustrate the ratio between the measurements in Fig. 3.4. Black lines show measurements recorded with a low-frequency network analyzer.

As explained in Sec. 3.2.4, we expect the modulation P_{th} of the thermal power dissipated in the core of the laser fiber to be proportional to the pump induced RI at low frequencies $f \ll f_r$. The thermal response to step changes in the self heating of erbium-doped amplifier fibers have earlier been calculated numerically in [24]. However, it is hard to deduce frequency responses over a broad frequency range from those results. We have calculated numerically the expected frequency response $\Delta\nu_{th}$ to a modulation of P_{th}. The impulse response to heating was calculated in the time domain by a finite element method. The calculated impulse response were Fourier-transformed to produce the frequency response. Parameters used in the calculations were: core diameter $d_{core} = 5.4$ μm; mode field diameter $MFD = 5.8$ μm (Gaussian distribution); fiber diameter $d = 80$ μm; thermal conductivity $k_c = 1.37$ W/(m K); diffusivity $D = 0.82 \times 10^{-6}$ m^2/s; and fiber thermooptic coefficient $\delta n/(n\delta T) = 5.2 \times 10^{-6}$ K^{-1}. We believe that these parameters are representative for the investigated fiber.

The gray lines in Fig. 3.6 shows the calculated thermooptic frequency shift $r_{th} = \Delta\nu_{th}/RI$ fitted to the measurements by assuming a power dissipation

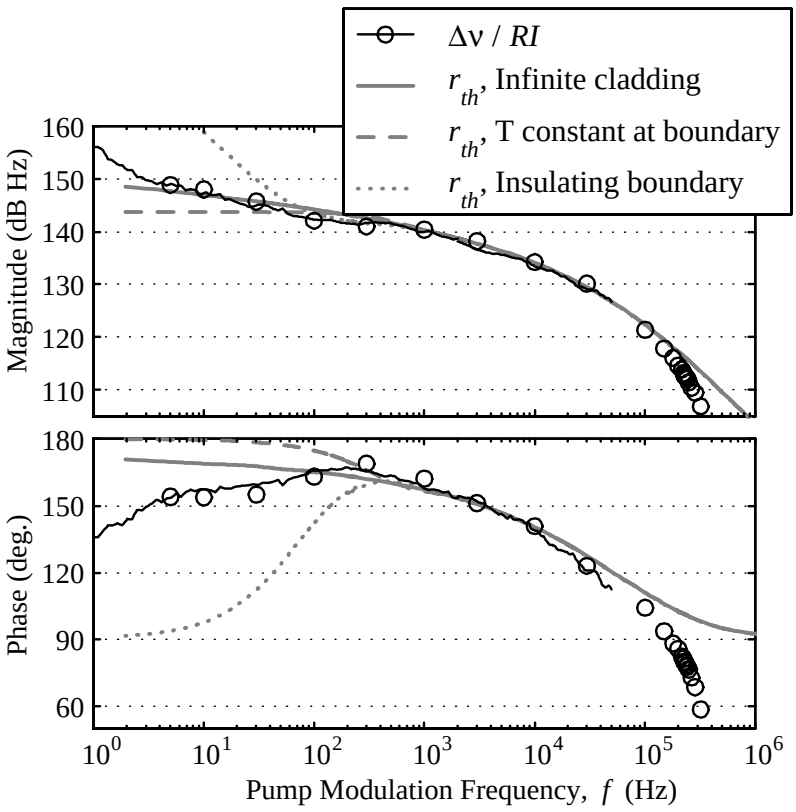

Figure 3.6. Black lines and circles: Ratio between the pump modulation responses $\Delta\nu$ and RI of the laser characterized in Fig. 3.4. Gray lines: Frequency response ν_{th} to 230 μW rms modulation of the heat absorbed in the core of a $L_c = 10$ mm long cavity, calculated for the fiber boundary conditions indicated in the legend text.

modulation amplitude of $RI \times 23$ mW/m. For a $L_c = 10$ mm laser cavity this corresponds to a dissipated power of $P_{th} = RI \times 230$ μW. If we assume that the thermal power dissipation is linear with intensity (as is verified for the fiber DFB laser investigated in Chap. 8), we may conclude that the DC thermal power dissipation in the laser cavity is close to 230 μW. The high value of the estimated P_{th} compared to the measured output power $P_o = 170$ μW indicates that power dissipation from the pumping process with ion relaxations to the upper laser level cannot be the dominating heating source. Remaining candidates are nonradiative absorption at the pump or laser wavelengths, due to some combination of saturable and non-saturable absorbers.

Three different simulated boundary conditions are illustrated in the figure, as indicated in the legend. The infinite cladding condition corresponds to immersing the laser into a medium with the same thermal properties (k_c and D) as silica. For the frequencies illustrated, the condition of constant temperature

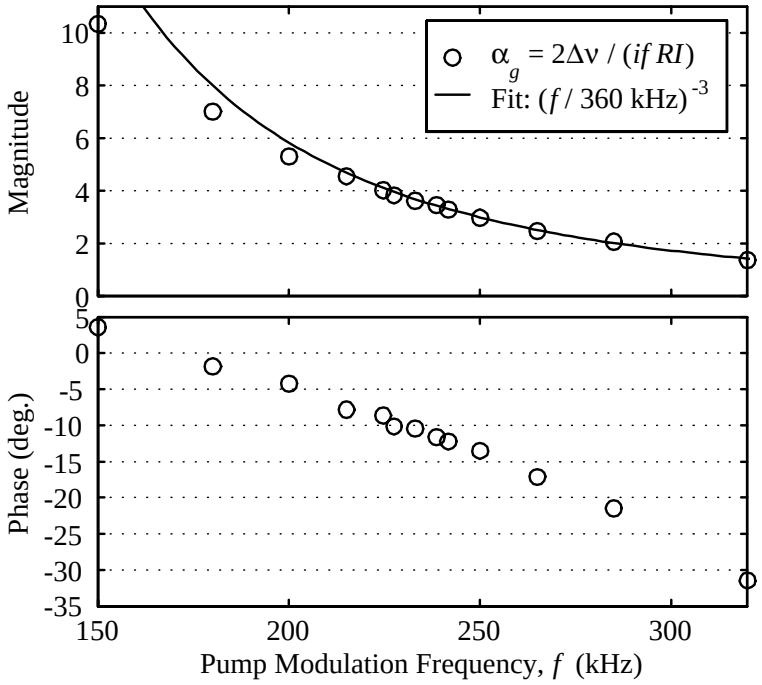

Figure 3.7. Circles: α_g according to (3.16) calculated from pump modulation measurements near the relaxation oscillation frequency $f_r = 238$ kHz. Line: Fit to a f^{-3}-dependence.

on the fiber surface should be a good approximation for a case where a good heat-sink (like aluminum) with high values for k_c and D is in contact with the fiber. The insulating boundary condition should approximate the effect of placing the fiber in a bad heat-sink such as air or a thick polymer coating. We see from the calculations that the boundary conditions become important for $f \lesssim 400$ Hz. The deviation between the measured response r_{th} and the calculated curves for $f < 400$ Hz in Fig. 3.6 are attributed to the thermal properties of the materials surrounding the fiber, which are not known. For 400 Hz $< f <$ 100 kHz, the agreement between measurements and calculations are reasonably good.

We see from Fig. 3.4 that the relaxation oscillation resonance starts to dominate the RI magnitude for $f > 100$ kHz. Fig. 3.7 shows the linewidth enhancement factor α_g near $f = f_r$ calculated according to (3.16) from the measured pump modulation responses in Fig. 3.4. The magnitude of $\alpha_g(f)$ fits well to an f^{-3} dependence in the frequency range $f = 200 - 320$ kHz, taking the value 3.5 at $f = f_r$. At lower frequencies a f^{-2} dependence is approached. The phase is about $-10°$ at $f = f_r$, decreasing with a slope of $-0.33°$/kHz. The observed frequency dependence of α_g cannot be described by a simple minimum-phase

model, and we are not able to determine which mechanisms (spectral hole-burning through the Kramer-Kronig relations, different thermal mechanisms) that dominate.

Fluctuations in the pump center wavelength will also lead to fluctuations in the pumping efficiency, due to the wavelength dependence of the pump absorption cross section. We believe that pump wavelength fluctuations can be modelled as an equivalent RIN_p. The spectral dependence of the pump absorption is especially pronounced near 975 nm in Er:Yb-fibers [25]. However, due to the relatively slow energy transfer from the pump absorption state of Yb to Er, having a single-pole low-pass frequency around $\sim$ 1 kHz [3], the sensitivity to fluctuations in the pump center wavelength is still expected to be moderate. With 1480-nm pumping the response of the gain medium is much faster, as demonstrated by Fig. 3.4. However, the wavelength dependence of the pump absorption is significantly lower than around 975 nm. Until recently, available fiber pig-tailed diode pump lasers have been multi-moded both around 975 and 1480 nm, with mode spacings typically in the 100 to 500 GHz range. Fluctuations in the relative intensity distribution between the modes of these lasers may be a significant source of fiber laser noise. 975-nm pump lasers that are stabilized by external fiber grating reflectors are now commercially available and widely used for low-noise fiber amplifiers. Grating-stabilized 1480-nm pump lasers (intended for wavelength multiplexing of multiple lasers to obtain high pump powers) have recently been advertized as new products on the market.

In single polarization fiber lasers, fluctuations in the pump polarization state will introduce noise through the polarization anisotropies of the individual gain ions. In Chap. 7 the magnitude of the pump polarization hole-burning effect is described by the parameter η_p. It follows from the theory in the appendix to Chap. 7 that changes of the pump polarization state launched into a single polarization laser from being orthogonal to parallel to the laser polarization is equivalent to a change in the pump power by the factor $1 + \eta_p$. For the dual polarization Er-Yb doped 1480-nm pumped fiber DFB lasers investigated in Chap. 7 we estimate $\eta_p = 0.021$.

If the fiber laser is used as a sensor element with remote pumping and interrogation through a long lead fiber, the changes in pump polarization state may potentially become quite rapid (Hz to kHz range), due to poor isolation against temperature changes and mechanical vibrations. A way of eliminating noise from pump polarization fluctuations would be by depolarizing the pump, for instance with an active polarization scrambler that modulates the pump polarization state at a frequency well above the relaxation oscillation frequency of the fiber laser.

3.6 Noise Measurements

We have characterized the relative intensity and optical frequency noise spectra for the fiber DFB laser that was characterized with respect to pump modulation in Sec. 3.5. The interrogation system used for the noise measurements is identical to the system for monitoring of the RI and $\Delta\nu$ described in Sec. 3.5. Simultaneously recorded traces for the RIN and ν_{rms} are shown as gray curves Fig. 3.8. In Fig. 3.8 we also show the pump intensity noise RIN_p and the electrical noise floor of the interrogation system when no light is incident on the detectors.

A number of sharp noise spikes is observed in the RIN spectrum between $f =$ 9.5 Hz and 640 Hz. This is believed mainly to be due to acoustic pick-up in the ~ 8 m lead fiber from the WDM to the fiber laser, modulating the polarization state of the pump, c.f. Sec. 3.5. Acoustical modulation of the polarization state of the signal reaching the interrogation system will also contributed to noise pick up, because of a small polarization dependence in the interrogation system originating from polarization dependent coupling ratios in the optical couplers used. The spikes in the measured RIN_p at 37, 50 100, and 150 Hz may also have originated from this kind of acoustical pick-up.[8]

Between $f = 10$ Hz and 30 kHz the measured RIN floor is essentially constant at -118 ± 1 dB Hz$^{-1/2}$. Shot noise according to (3.28), taking loss in the transmission from the laser to the detector into account, gives a RIN contribution of only about -145 dB Hz$^{-1/2}$. The dashed line in Fig. 3.8 (a) shows the spectral density $RIN = RIN_p T_p(f)$ expected according to (3.11, 3.13) to arise from a smoothened polynomial fit to the measured RIN_p. The parameters used are: $k_{slope} = 1.18$, $k_{s.abs} = 1.4 \times 10^{-5}$ (taken from the measurements in Sec. 3.5); $\tau_{rt} = 1 \times 10^{-10}$ s ($\Leftrightarrow L_c = 10$ mm, which is a typical number for Ionas lasers); as well as the fitted parameters $f_r = 222$ kHz, and $f_{sat} = 51$ kHz. We see that the pump-induced RIN is ~ 5 dB lower than the measured RIN, indicating that other noise sources are dominating. Remaining candidates are fluctuations in the pump center wavelength λ_p, loss modulation Δa_{rt}, and spontaneous emission e_{sp}.

The dotted line in Fig. 3.8 (a) shows the spectrum $RIN = [RIN_p^2 T_p^2(f) + k_0 T_{loss}^2(f)]^{1/2}$ expected to arise from the measured RIN_p combined with white noise modulation of Δa_{rt} and e_{sp} described by the fitted parameter $k_0 = \Delta a_{rt}^2 + 4Me_{sp}^2/P_o = 8 \times 10^{-20}$. The fit to the RIN measurement is good.

The ratio ν_{rms}/RIN of the measured noise spectral densities in Figs. 3.8 (a) and (b) is illustrated by the black curve in Fig. 3.9. For comparison, The

[8] Fans and transformers in the laboratory instruments tend to produce vibrations at frequencies that are multiples of the 50 Hz line frequency.

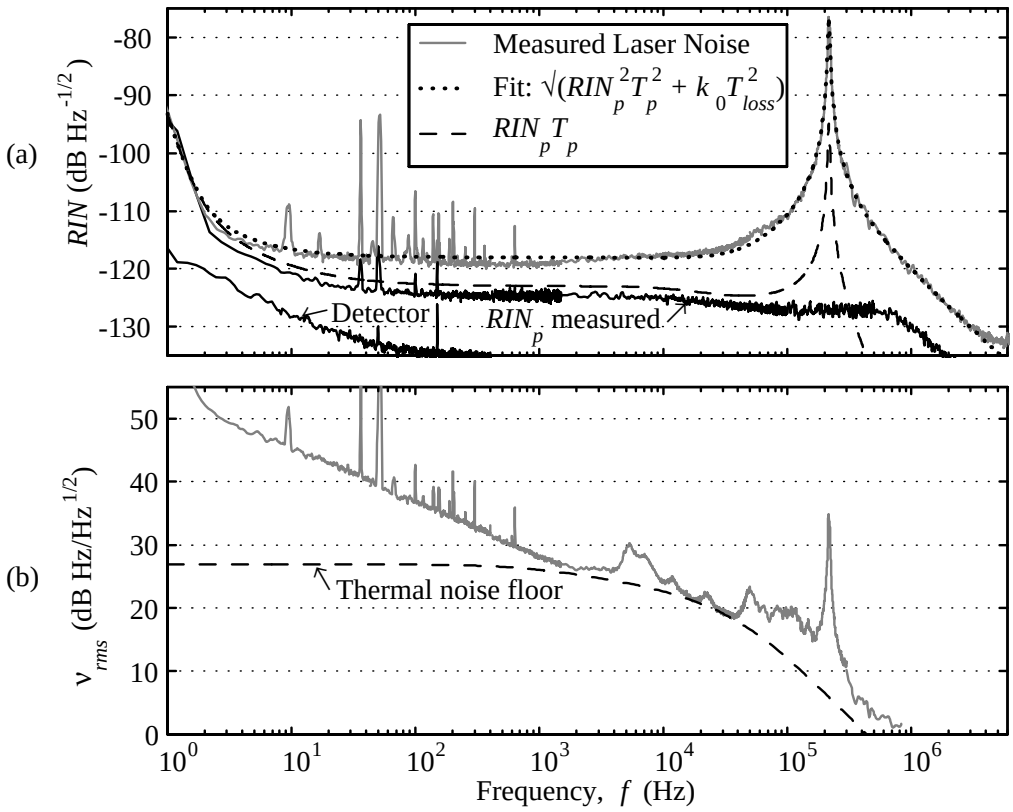

Figure 3.8. Solid gray curves in (a) and (b): fiber DFB laser RIN and ν_{rms} spectra, respectively. Solid black curves in (a): measured RIN_p and noise from detector electronics. Dashed and dotted lines in (a): expected noise from RIN_p only, and from a combination of RIN_p, Δrtl, and e_{sp}. Dashed line in (b): expected thermal noise according to (3.33, 3.34) with 6 dB added for conformity with reported experiments, using $L_c = 10$.

ratio $\Delta\nu/RI$ measured in the pump modulation experiment in Sec. 3.5 is indicated by open circles. The complex quantity $\langle\Delta\nu RI\rangle^*/RIN^2$ is also illustrated. $\langle\Delta\nu RI\rangle^*/RIN^2$ can be interpreted as the transfer function from the RI to the correlated component of $\Delta\nu$. (It may be useful in this context to recall the definitions $\nu_{rms}^2 = \langle\Delta\nu^2\rangle$ and $RIN^2 = \langle RI^2\rangle$.)

For frequencies below 100 kHz the measured $|\langle\Delta\nu RI^*\rangle/RIN^2|$ is typically 15 to 20 dB lower than ν_{rms}/RIN. This difference implies that only a $1-3$ % fraction of the frequency noise power ν_{rms}^2 originates from (is correlated with) the RIN.

If the laser RIN originated only from the effective value of RIN_p (including effects of pump wavelength fluctuations), $|\langle\Delta\nu RI^*\rangle/RIN^2|$ would equal the pump-induced $\Delta\nu/RI$ in Fig. 3.9. However, the measured $|\langle\Delta\nu RI^*\rangle/RIN^2|$ is

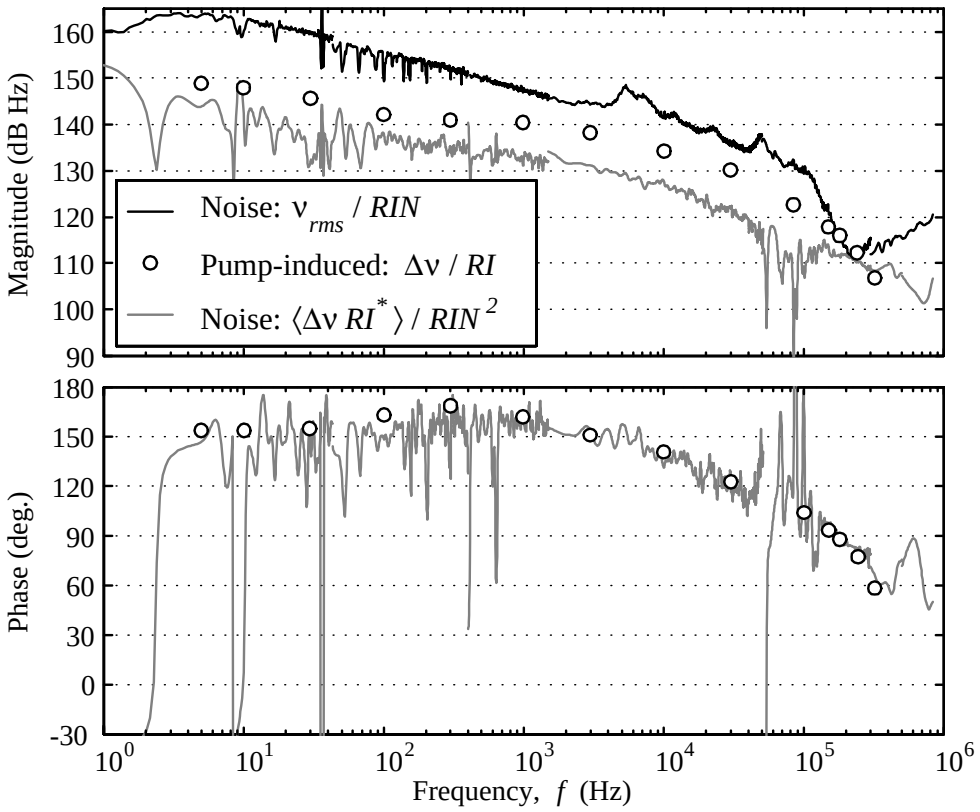

Figure 3.9. Ratio ν_{rms}/RIN from noise measurements; $\Delta\nu/RI$ from pump modulation response measurements; and "transfer function" $|\langle\Delta\nu RI^*\rangle/RIN^2|$ between the correlated components of RI and $\Delta\nu$ from the noise measurements.

4 to 9 dB lower than the pump-induced $\Delta\nu/RI$ at frequencies $f < 100$ kHz. The difference equals (to within the measurement accuracy) the difference observed in Fig. 3.8 (a) between the measured RIN and the calculated RIN_pT_p. This observation indicates that the difference between the measured RIN and the calculated RIN_pT_p originates from a noise source that produces frequency and intensity noise components with a ratio $\Delta\nu/RI$ that is far below the pump-induced $\Delta\nu/RI$. In other words, r_{th} (3.17) seems to be smaller for noise induced by random cavity loss modulation Δa_{rt} or spontaneous emission e_{sp} than for pump-induced noise. This verifies that pump wavelength fluctuations cannot be the origin of the measured excess RIN above RIN_pT_p in Fig. 3.8 (a). We are left with the candidates Δa_{rt} and e_{sp}.

The spontaneous emission power density from the fiber laser (outside the grating stop-band) was measured at threshold to be 3.5×10^{-21} W/Hz ± 2 dB. The spontaneous emission per unit length of fiber inside the laser cavity is not

expected to change significantly above threshold. Assuming a total Er-doped fiber length of ~ 60 mm we can thus estimate the spontaneous emission power launched into the laser mode as $e_{sp}^2 = 2L_c \times (3.5 \times 10^{-21}$ W/Hz$)/(60$ mm$) = 1.2 \times 10^{-21}$ W/Hz ± 2 dB. If the estimated $k_0 = 8.8 \times 10^{-20}$ in Fig. 3.8 originates only from spontaneous emission noise, with no significant contribution from loss modulation ($\Delta a_{rt} \approx 0$), then the estimated e_{sp}^2 corresponds to a laser mirror transmissivity of $M = k_0 P_o/(4e_{sp}^2) \approx -25 \pm 2$ dB. This corresponds to an effective κL of 7.2 ± 0.5, which is fairly low but still possible. If the loss modulation contributes significantly to the RIN, the value of κL may be much higher. A possible source of loss modulation could be random fluctuations in the saturable absorber inversion, for instance due to the shot-noise originating from quantization of the absorbed energy into photons.

The dashed line in Fig. 3.8 (b) shows the thermal noise floor according to Wansers formula (3.33, 3.34), using $L_c = 10$ mm, with 6 dB added (c.f. Sec. 3.3) for conformity with previously reported experiments. We see that the measured ν_{rms} touches down to this floor in several regions between 1 and 50 kHz. The noise peak in ν_{rms} between 4 and 15 kHz is believed to be due to acoustical noise in the lab. The small peak at 48 kHz coincides in frequency with the 1st order resonance of the PZT optical phase modulator in the interferometer. We do not know the explanation for the general increase compared to the predicted thermal noise for $f > 50$ kHz.

For $f < 1$ kHz a $1/f$ component is observed in ν_{rms}, with a slope of -8.6 dB per decade in f. The origin of this noise component is not understood. A similar $1/f$ noise component was observed in the beat frequency noise spectrum of a dual polarization fiber DFB laser characterized in Chap. 7.

A sharp increase in ν_{rms} can be observed near the relaxation oscillation frequency in Fig. 3.8 (b). This noise peak originates from the relaxation oscillation peak in the RIN spectrum, via the linewidth enhancement factor α_g. In Fig. 3.9 we see that the ratio of the rms noise magnitudes ν_{rms}/RIN, the pump-induced ratio $\Delta\nu/RI$, and the noise "transfer function" $|\langle \Delta\nu RI^* \rangle / RIN^2|$ become essentially equal near $f = f_r$. This is as expected from the discussion in Sec. 3.2.4 of α_g near $f = f_r$ according to (3.16).

The total optical power detected from the interferometer was $\sim 8\ \mu$W, giving a shot noise equivalent frequency shift (3.29) at the investigated frequencies $f < 850$ kHz of $NE\nu \approx -22$ dB Hz$/\sqrt{\text{Hz}}$.

Fig. 3.10 shows a summary of the measured and theoretical frequency noise limits for the fiber DFB laser investigated in this section. The thermal noise curve is identical to that in Fig. 3.8 (b). The spontaneous emission noise is estimated from (3.25), with $e_{sp}^2 = 1.2 \times 10^{-21}$ W/Hz, $\tau_{rt} = 1 \times 10^{-10}$, $P_o = |A|^2 = 170\ \mu$W, $M = -25$ dB ($\kappa L = 7.2$), and $\alpha_g = 3$. The illustrated spontaneous emission noise floor should be regarded only as an indication of

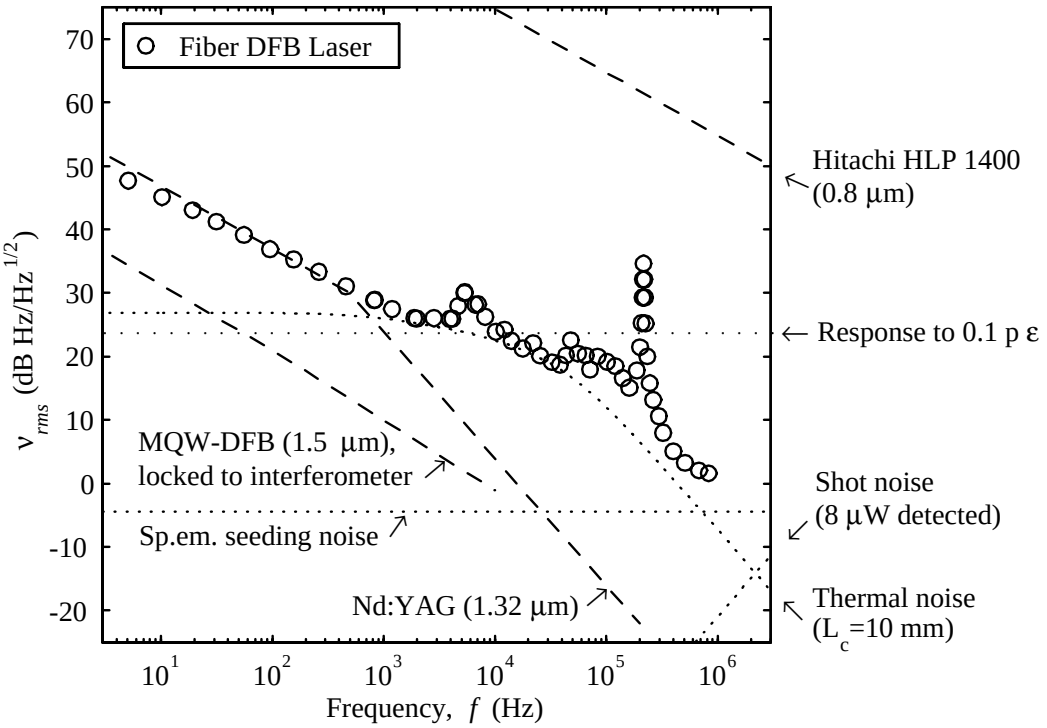

Figure 3.10. Sumary of measured and theoretical limits to ν_{rms}. Dotted lines illustrate the esitimated fundamental shot noise (3.30), thermal noise, and estimated spontaneous emission noise. Dashed lines: Published noise levels of a common 800 nm semiconductor laser, a Nd:Yag ring laser, and a tunable semiconductor MQW laser with active frequency stabilization.

the order of magnitude, since M and α_g are not known for this specific laser. If we assume $M = -46$ dB (corresponding to $\kappa L = 12$), the shot noise estimate decreases by 21 dB to -25.5 dB Hz/$\sqrt{\text{Hz}}$.

For comparison, results published for a relatively inexpensive 800 nm semiconductor laser [23], a tunable multiple quantum well (MQW) semiconductor DFB laser applying active frequency stabilization by feedback from an interferometer [26], and a Nd:YAG ring laser [1, 23] are also shown in the figure. We see that the $1/f$ noise level of the Nd:YAG laser is very similar to that of the fiber laser. The performance of the interferometer-locked MQW laser below 10 kHz is generally 15 dB better than that of the fiber DFB laser. It should be possible to obtain even better performances by locking a fiber DFB laser to a fiber interferometer.

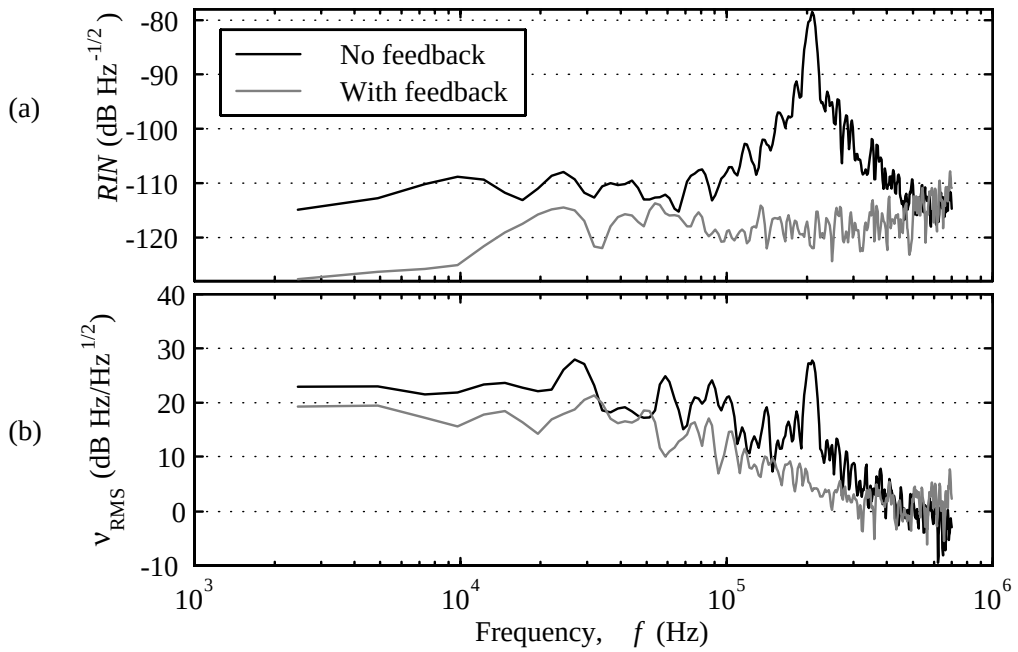

Figure 3.11. (a) RIN and (b) frequency noise ν_{rms} of a fiber DFB laser with and without RIN to pump feedback stabilization.

3.7 Noise Reduction by Feedback to the Pump Laser

RIN reduction for a single frequency Er-doped fiber Bragg grating laser by applying negative feedback from a monitor detector to the pump current has earlier been demonstrated in [27, 28]. To be able to investigate what happens to the laser frequency noise when such feedback is applied, we implemented a PID (proportional gain - integrator - differentiator) controller of the same type as used in [27] in a feedback path from the monitor detector to the pump drive current.

Fig. 3.11 shows the RIN and frequency noise ν_{rms} from a 50 mm long Ionas fiber DFB laser (not identical, but similar to the one investigated in the previous sections) which was pumped by ~ 110 mW of 1480-nm power. The noise spectra were measured both for the cases with and without feedback to the pump. We see from Fig. 3.11 (a) that the relaxation oscillation peak near $f_r = 206$ kHz is effectively removed by the feedback. The RIN noise floor of ~ -118 dB Hz$^{-1/2}$ obtained with the feedback circuit is limited by noise generated in the monitor detector. With a better detector design we believe that the RIN would be limited by the shot noise at the monitor detector, which in our case with ~ 50 μW of detected power would be -143 dB Hz$^{-1/2}$.

From Fig. 3.11 (b) we see that the relaxation oscillation peak in the frequency noise spectrum is also removed efficiently by the feedback. A small reduction in ν_{rms} by ~ 2.5 dB is also observed for $f \lesssim 300$ kHz. We have not verified whether this noise reduction is a consequence of the feedback, or if it is only due to random fluctuations in the measurements. If the noise reduction is due the feedback, then this indicates that the contribution from pump noise to both RIN and ν_{rms} of the free running laser is more dominant for the present laser than for the laser investigated in the previous sections.

The ratio ν_{rms}/RIN of the free running laser in Fig. 3.11 at the relaxation oscillation peak $f_r = 206$ kHz equals 106.5 dB Hz. By inserting this ratio into (3.16) we estimate the effective linewidth enhancement factor at $f = f_r$ to be $\alpha_g \approx 2.1$ for this laser.

3.8 A Serially Multiplexed Fiber DFB laser Array

3.8.1 Introduction

An array with four serially multiplexed fiber DFB lasers pumped at 1480nm has been tested and evaluated at Optoplan with respect to output frequency noise and RIN noise. The array was on loan from Ionas AS in Denmark, and should be similar to the array investigated in [29]. A sensor laser array with 4 serially multiplexed single frequency Er-doped fiber lasers has earlier been demonstrated in [30]. We here present a more detailed characterization of the noise performance of the Ionas laser array, and investigate the effect of applying feedback to the pump from a detector that monitors the output from the array.[9]

The pump absorption in Er^{3+}-doped fiber DFB lasers pumped at 1480 nm can in principle be well below 0.05 dB (1.2 %), provided that splice losses do not dominate. This allows for serial multiplexing of a large number of fiber DFB lasers operating at different wavelengths, provided that interactions or reflections between the lasers do not make the laser operation unstable. Serial multiplexing of lasers is interesting both for multiplexing of fiber laser sensors and for making compact, low cost, and accurate multiple wavelength sources.

As mentioned in Secs. 3.2.3 and 3.2.4, back-reflections from external reflectors can degrade the laser stability. Back reflections may be caused by other fiber components, connectors, grating side-bands of serially multiplexed fiber DFB lasers, or by Rayleigh scattering. This constitutes a problem if one wants to create multiplexed fiber DFB laser sensor systems that are distributed over large distances (> 30 to 300 m).

[9] This section is based on the Optoplan Report: "Test of Ionas fiber DFB laser array".

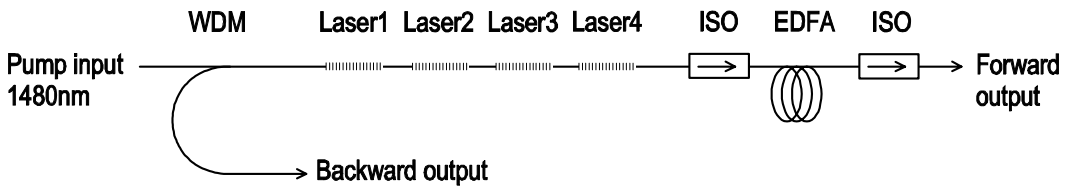

Figure 3.12. Laser array system on loan from Ionas AS. WDM, wavelength division multiplexer; ISO, optical isolator; EDFA erbium doped fiber amplifier.

We show in Chapters 4 and 5 that the tolerance to reflections from short distances ($\lesssim 10$ m) is reasonably high. This is promising for the possibilities of making a multiwavelength fiber DFB laser source without having to introduce isolators or attenuators between the lasers. However, one may suspect that the effect of having the power from each laser passing through all the other lasers, contributing to each others gain saturation, might introduce excess noise. Intensity noise in one laser may also be propagated to lasers further away from the pump via fluctuations in the pump absorption of the first laser. One may also fear that feedback mechanisms between the laser intensities could make the whole system start self-oscillating. One way of avoiding high feedback gains would be to make the outputs from each laser highly directional in the same direction as the pump by introducing asymmetries in the laser gratings. This type of configuration is used for the laser array investigated below.

It would be attractive if one was able to reduce the output RIN from the individual lasers in a fiber DFB laser array by applying feedback to the pump in a way similar to that demonstrated in Sec. 3.7. One may argue that it must be hard to control a multiple of independent signals (the RI of multiple lasers) by modulation of only one parameter (RI_p). We will here take a simple approach to the problem. Although we do not succeed in removing RIN from the array lasers, the results may provide some insight into the dynamics of the feedback system.

3.8.2 The Investigated Array

The laser array system contained four serially multiplexed Er-doped fiber DFB lasers, a 1480 / 1550 nm WDM, and an EDFA to boost the forward output power. Fig. 3.12 shows the system configuration. The WDM and the DFB lasers were packaged in a sealed box. The pump input port was spliced to a 1480nm diode laser with controller electronics built at Optoplan. The pump controller had options for either constant current operation or stabilization of the power from the fiber lasers by negative feedback via a PID-controller from a monitor detector to the pump laser. The monitor detector could either be connected to the forward or to the backward output ports from the array.

Laser1/2	$\lambda 1 = 1551.1$ nm
Laser1/2	$\lambda 2 = 1549.3$ nm
Laser3	$\lambda 3 = 1548.5$ nm
Laser4	$\lambda 4 = 1550.9$ nm

Table 3.1. Overview of the characterized lasers.

The laser wavelengths and the order of the lasers in the array, as specified from Ionas, is given in Tab. 3.1. The order of the first two lasers ($\lambda 1$ and $\lambda 2$) is not known.

3.8.3 Interrogation System

The wavelength demultiplexer system used to pick out the individual laser wavelengths received from the array is shown in Fig. 3.13. Two fibers with uniform Bragg gratings FBG1 and FBG2 inscribed were each mounted between a fixed point and a manual translation stage, allowing for independent strain-tuning of the grating center wavelengths. The strained lengths were between 50 and 70 cm. The position of the translation stages could be monitored on dial position meters. FBG1 was fixed with tape on an aluminum cylinder at each end, assisted by the friction of a few turns around the cylinders. The tuning repeatability for this grating was not very good (about ± 50 pm), probably because the fiber was slipping on the cylinders. FBG2 was mounted with acrylate glue, resulting in better tuning repeatability.

When the grating stop band was strain-tuned over the laser wavelengths, fringes with peak-to peak amplitudes of 3 to 10 % of the DC level could be observed at the detector. This is probably due to reflections from the output detectors, implying that acoustically or thermally induced noise in the output fiber lengths may have induced extra RIN at the detectors. The influence of such acoustical and thermal noise is believed to be negligible at high frequencies. FBG1 could be tuned over the wavelengths $\lambda 1$, $\lambda 2$ or $\lambda 3$. FBG2 could be tuned to $\lambda 1$ or $\lambda 4$. In this way any two lasers could be monitored at the same time.

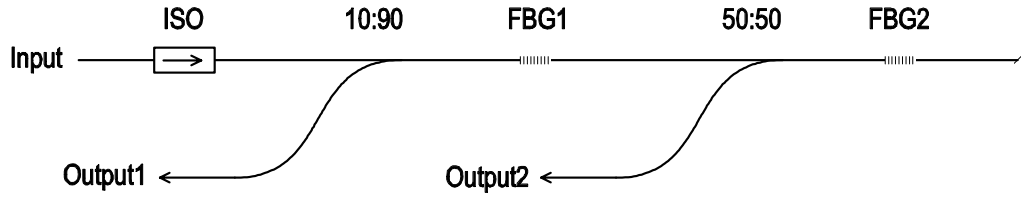

Figure 3.13. Wavelength demultiplexer. ISO, optical isolator; FBG1 and FBG2, strain tuned fiber Bragg gratings.

One of the two outputs from the demultiplexer was split by a 50:50 coupler and guided to a detector for RIN monitoring and to a Mach-Zehnder interferometer (MZ) with balanced detection for optical frequency noise monitoring. Active feedback to a PZT ring in one of the MZ arms was used to keep the DC interference phase in quadrature.

3.8.4 Output Power

With $\sim$ 140 mW of pump power entering the WDM, the total power from the forward output of the array was $\sim$ 10 mW. By inserting an optical band-pass filter (90 nm bandwidth) between the forward output and the detector it was verified that remaining pump power constituted less than 20 % of this power.

Tab. 3.2 shows the relative forward output powers from the different lasers, measured with the wavelength demultiplexer in Fig. 3.13.

The total backward output power with $\sim$ 140 mW pump was measured to $\sim$ 26 μW. According to Ionas, the lasers do not have equal output powers in both directions, and they are mounted such that they will give their maximum output power in the forward direction. This explains the low backward output power.

3.8.5 Performance without Feedback to the Pump

The RIN and frequency noise of the individual lasers were first measured with pump laser driver in a constant current mode. The pump power was set close to its maximum value of 140 mW. For each wavelength, the RIN and frequency noise spectra were recorded simultaneously. The results are shown in Fig. 3.14.

The relaxation oscillation resonance frequency f_r, the RIN and ν_{rms} at $f = f_r$, and the estimated α_g at $f = f_r$ according to (3.16) for each laser are summarized in Tab. 3.3. The lower peak noise densities for $\lambda 2$ compared to the other laser wavelengths may be explained by the lower Q-factor (inverse relative bandwidth) of the relaxation oscillation resonance in this laser compared to the others. For a given driving noise source (from pump fluctuations, vibrating back-reflectors etc.) the output peak noise power density should be proportional

Wavelength	Normalized output power (a.u.)
$\lambda 1$	1
$\lambda 2$	0.91
$\lambda 3$	0.66
$\lambda 4$	0.79

Table 3.2. Relative output powers.

Wavelength	f_r (kHz)	$RIN(f_r)$ (dB Hz$^{-1/2}$)	$\nu_{rms}(f_r)$ (dB Hz/$\sqrt{\text{Hz}}$)	α_g at $f = f_r$
$\lambda 1$	166	-74.8	33.0	2.4
$\lambda 2$	345	-85.3	27.6	2.6
$\lambda 3$	205	-70.0	31.5	3.8
$\lambda 4$	212	-74.6	37.2	3.6

Table 3.3. f_r, as well as RIN, ν_{rms}, and estimated α_g at $f = f_r$ for each laser wavelength

to the resonance Q-factor. If the resonances are affected by feedback between the intensities of the individual lasers, the lower Q-factor for $\lambda 2$ could be related to its large spacing in resonance frequency from the other lasers. It could also be related to its position as one of the first two lasers in the array counted from the pump input, since the first laser does not experience pump fluctuations caused by RIN fluctuations in lasers that are closer to he pump. However, a likely explanation for the variations in Q-factor is variations in the Q-factors of the solitary lasers (without effects of feedback).

3.8.6 Performance with Feedback to the Pump

Fig. 3.15 shows the RIN noise measured from the forward output when negative feedback was applied to the pump via the PID-controller. Again, the pump power was kept close to 140 mW. Both feedback from the forward [Fig. 3.15 (a)] and the backward [Fig. 3.15 (b)] outputs were investigated. In the latter case, the electronic gain of the feedback controller was increased by a factor of 71 compared to the former case, in order to partly compensate for the reduced DC power at the monitor detector. The dashed line shows the RIN noise at the feedback monitor detector. The peak in the monitor spectrum near 500 kHz is du to a relatively low stability phase margin of the electronic feedback loop.

By comparing Figs. 3.14 and 3.15 one see that the main effect of the feedback is to distribute the RIN-noise between the lasers. That is: When one laser oscillates at its resonance frequency, the feedback compensates in such a way that all four lasers starts oscillating at this frequency, but with such phases and amplitudes that the total monitor power is stabilized. Consequently, there is no significant overall improvement in the individual RIN noise levels due to the feedback. It is interesting, however, to observe that the relaxation oscillations of the laser $\lambda 2$ has been reduced very effectively by the feedback. This may be because of the relatively large separation of the relaxation oscillation frequency of this laser from the other resonance frequencies, meaning that the remaining three lasers are relatively insensitive to the feedback modulation of the pump power at the relaxation oscillation frequency of $\lambda 2$.

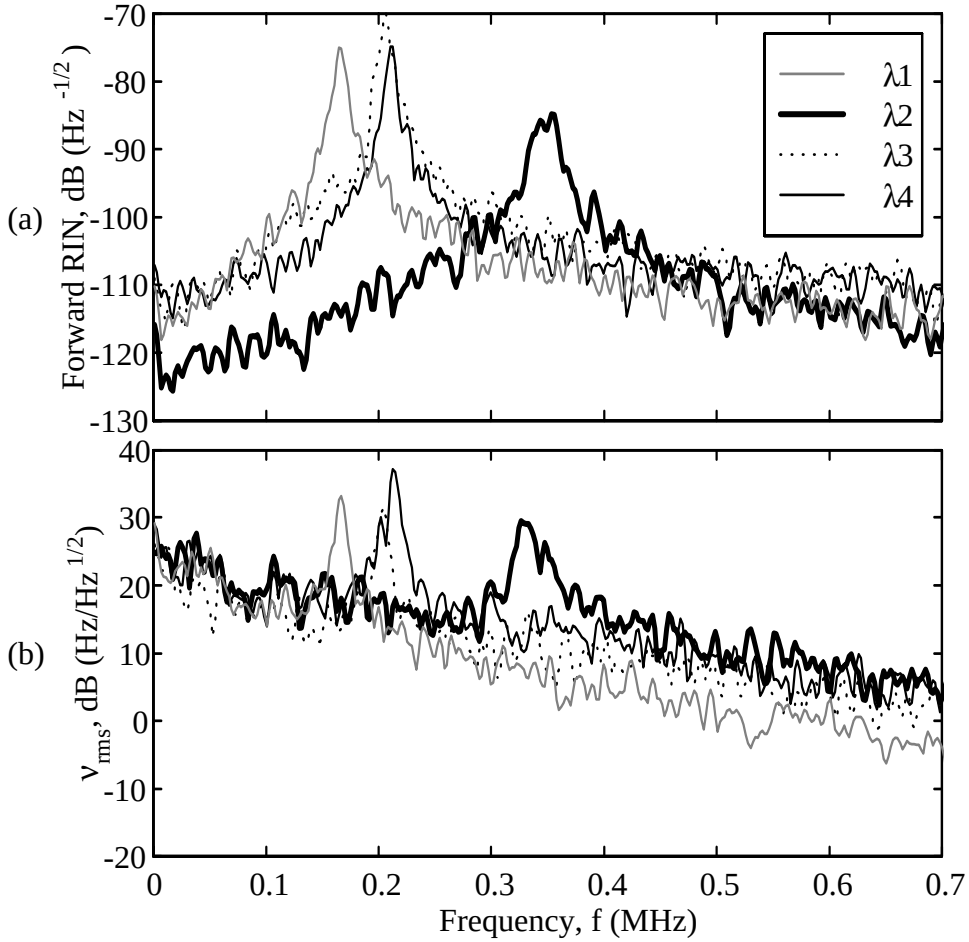

Figure 3.14. (a) RIN and (b) Frequency noise from the array lasers without feedback to the pump. The noise was measured from the forward output of the array.

The RIN at low frequencies of individual lasers with active feedback to the pump was also investigated. When feedback from the forward output was used, no striking noise phenomena could be observed (except for interference effects in the wavelength demultiplexer). However, when the feedback monitor was connected to the backward output, the forward output power was found to make abrupt changes by 10 to 15 % in amplitude at intervals of 1 to 10 s. The power changes occurred simultaneously and with the same sign at all laser wavelengths. The reason for this behavior is believed to be sudden changes in the lasing efficiency (or the forward to backward output ratio) of individual lasers. Such changes will cause the feedback electronics to change the pump power so that the backward output power is kept constant. This will, how-

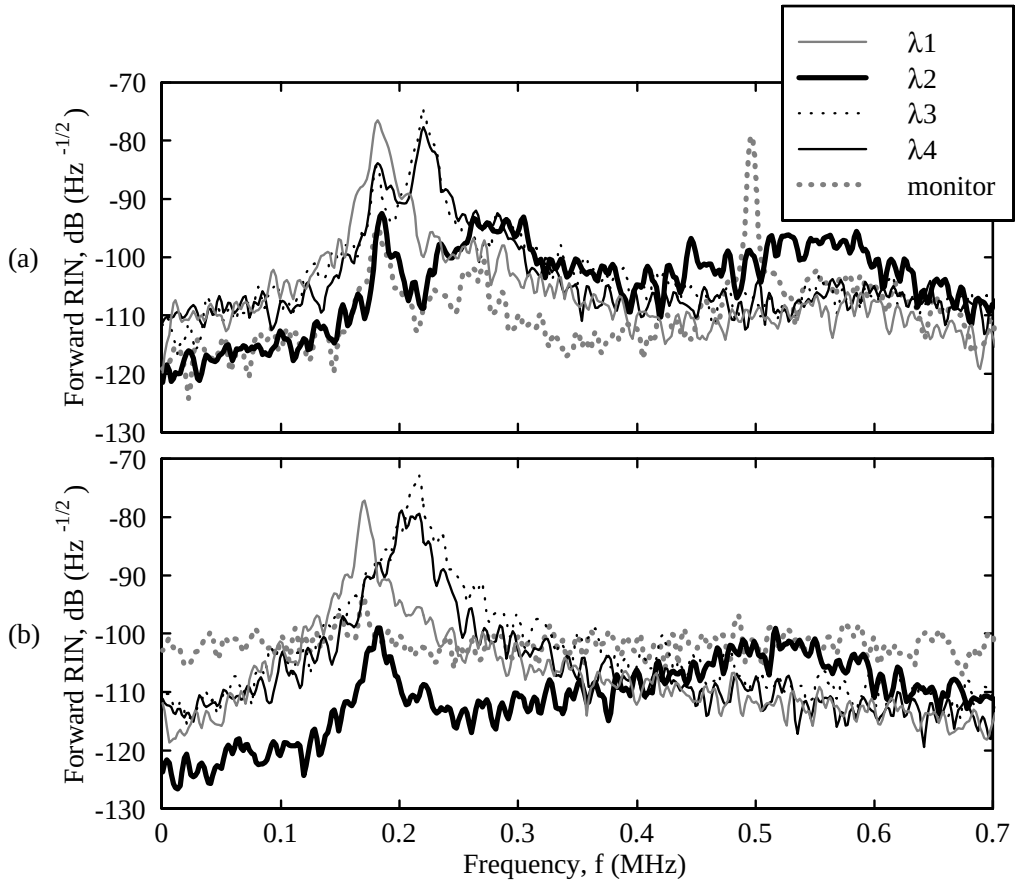

Figure 3.15. RIN with feedback to the pump from the (a) forward and (b) backward outputs of the array. The RIN of each laser was measured from the forward output of the array. The total RIN at the monitor detector is also illustrated.

ever, also cause changes in the remaining pump available for the EDFA, and amplification of the forward output changes for all wavelengths.

Fig. 3.16 shows the laser frequency noise measured with feedback to the backward output. Each of the spectra in Fig. 3.16 was measured simultaneously with the corresponding RIN spectrum in Fig 3.15 (b).

One may compare the noise measurements in Figs. 3.14 through 3.16 with the noise levels in Fig. 3.11 of a typical non-multiplexed Ionas fiber DFB laser with and without feedback to the pump. We see that without feedback to the pump, the RIN and frequency noise levels are similar for the single laser and the multiplexed lasers is Fig. 3.14. When feedback is applied, the RIN is dramatically reduced for the single laser, accompanied by a removal of the relaxation oscillation noise peak in ν_{rms}. This noise reduction is not achieved for the multiplexed lasers in Fig. 3.15.

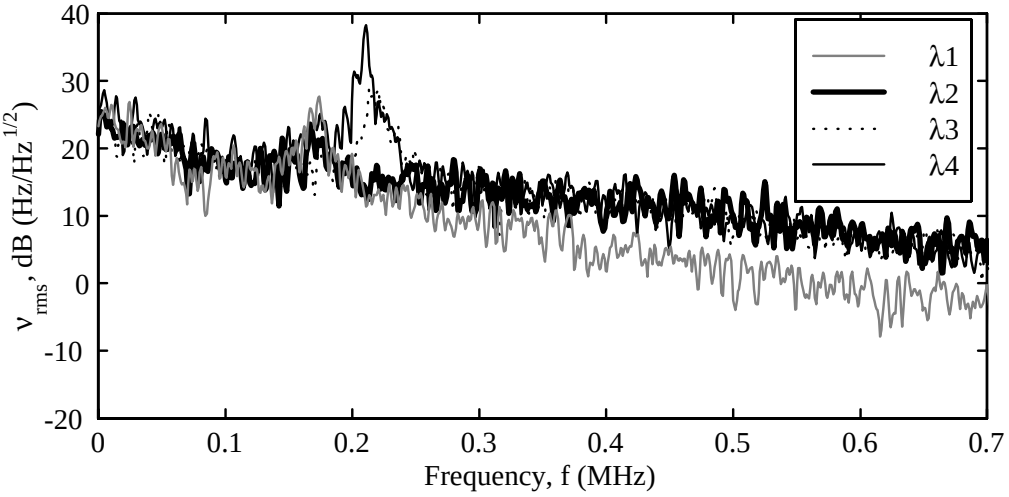

Figure 3.16. Frequency noise with feedback from the backward output of the array to the pump.

3.9 Conclusion

The origins of relative intensity noise RIN and optical frequency noise ν_{rms} in fiber DFB lasers has been studied both theoretically and experimentally. The correlation between intensity and frequency fluctuations has also been studied, in terms of the linewidth enhancement factor α_g and the self heating coefficient r_{th}.

The measured RIN ranges from a typical level of -118 dB Hz$^{-1/2}$ between $f = 10$ Hz and 30 kHz to a maximum of -78 dB Hz$^{-1/2}$ at the relaxation oscillation frequency f_r, and seems to be dominated either by random fluctuations in the cavity losses (possibly due to fluctuations in the saturable absorption), by spontaneous emission noise, or by a combination of the two noise sources. f_r varies between the investigated lasers from 166 to 345 kHz. Calculations indicate that the spontaneous emission induced noise (both RIN and ν_{rms}) can be reduced to negligible levels (3.22) if the laser mirror transmissivities are sufficiently low (effective $\kappa L \gtrsim 10$). Unfortunately, we do not know the mirror transmissivities for the investigated lasers.

A fundamental source of laser frequency noise ν_{rms} seems to be the random diffusion of thermal energy within the fiber cross-section. Above $f = 1$ kHz, except for near $f = f_r$, the measured ν_{rms} is typically 0 to 6 dB above the thermal noise floor expected from measurements of fiber interferometer noise published in [22, 23, 5, 21]. For a fiber DFB laser with a 10 mm effective cavity length, the expected thermal noise floor decreases from ~ 25 dB Hz/$\sqrt{\text{Hz}}$ at $f = 1$ kHz to ~ -5 dB Hz/$\sqrt{\text{Hz}}$ 1 MHz. The measured increase above this

floor for $f \lesssim 50$ kHz is believed to be due to acoustical noise. Above $f = 50$ kHz, the origin of the excess noise is more unclear.

For $f < 1$ kHz an $1/f$ component is observed in ν_{rms}, which is qualitatively similar to the polarization beat frequency noise observed in Chap. 8 for a different laser. The origin of the $1/f$ noise has not been identified.

Near $f = f_r$ the optical frequency and intensity fluctuations are found to be highly correlated, and related by the linewidth enhancement factor $\alpha_g \simeq 2\nu_{rms}/(f\,RIN)$. A low value of α_g is thus desirable in order to reduce $\nu_{rms}(f_r)$. Low values of α_g are also expected to improve the lasers tolerance to external reflections, as will be further discussed in Chaps 4 and 5. Our measured values for α_g at $f = f_r$ range from 2.1 to 3.8, as compared to typically from 3 to 7 for semiconductor lasers. To our knowledge, this is the first time that values for α_g in a fiber laser is reported experimentally. Calculations reported in [13] (not including possible thermal contributions to α_g) indicate that α_g will depend strongly on the laser wavelength, going through zero somewhere near 1540 nm. α_g is also expected to depend on a number of other parameters, such as frequency f, pump power, and saturating signal power in the cavity (which is strongly dependent on κL). We observed a strong decrease in α_g with increasing f within the relaxation oscillation ~ 25 dB bandwidth from 170 to 270 kHz..

At frequencies well below f_r the only laser noise contributions that depend on α_g are spontaneous emission induced frequency noise and noise due to cold cavity loss fluctuations. The coupling to ν_{rms} from RIN components that are induced by loss fluctuations or pump noise is believed to be dominated by thermal effects at these frequencies.

By comparing the pump modulation responses of the laser output power and the optical frequency shift we have determined the frequency response $r_{th}(f)$ of the Er-doped fiber to self heating from power dissipation in the core at frequencies below the relaxation oscillation peak ($f \lesssim 180$ kHz). Good agreement with theoretical calculations was found for $f > 400$ Hz. The theory shows that the fiber boundary conditions (heat sink), which were not known for the investigated fiber, are of great importance at lower frequencies.

The spontaneous emission induced frequency noise in fiber DFB lasers is typically many orders of magnitude smaller than in semiconductor lasers, due to the much lower effective laser mirror transmissivities and longer cavity roundtrip delays. Other noise sources, such as thermal fluctuations, are found to dominate in fiber DFB lasers. The huge difference in spontaneous emission noise levels explains why fiber DFB lasers have linewidths that are much smaller than semiconductor lasers.

We have verified that active stabilization of the laser RIN by feedback to the pump laser from a detector monitoring the fiber laser output power effec-

tively removes the relaxation oscillation peak from the optical frequency noise spectrum.

The observation that single polarization fiber DFB lasers can be multiplexed along a single fiber with a common pump without significant degradation of the noise performance is promising for the possibility of performing multiple point distributed sensing with fiber DFB lasers. It is also promising for the possibility of making compact, low cost, and accurate multiple wavelength sources.

3.10 Acknowledgments

The author acknowledges Dag Thingbø at Optoplan AS for contributions to the design and implementation of the electronic circuits used in the experiments, and especially for designing and implementing the feedback circuit used in Secs. 3.7 and 3.8. Thanks go also to Jon Thomas Kringlebotn, Kjell Bløtekjær, Dag Roar Hjelme, and Sigurd Løvseth for inspiring and stimulating discussions, and for reading through and commenting on this manuscript, and to Ionas for lending us their laser array.

References

[1] K. J. Williams, A. Dandridge, A. D. Kersey, J. F. Weller, A. M. Yurek, and A. B. Tveten, "Interferometric measurement of low frequency phase noise characteristics of a diode pumped Nd:Yag ring laser", Electron Lett., Vol. 25, p. 774, 1989.

[2] T. L. Boyd, D. Klemer, P. A. Leilabady, J. Noriega, and M. Pessot, "A 1.55-μm Solid-State Laser Source for DWDM Applications", J. of Lightwave Tech., Vol. 17, pp. 1904–1908, 1999.

[3] S. Taccheo, P. Laporta, O. Svelto, and G. De Geronimi, "Intensity noise reduction in a single-frequency ytterbium-codoped erbium laser", Opt. Lett., Vol. 21, pp. 1747–1749, 1996.

[4] J. T. Kringlebotn, W. H. Loh and R. I. Laming, "Polarimetric Er^{3+}-doped fiber distributed-feedback laser sensor for differential pressure and force measurements", Opt. Letters, Vol.21, pp.1869–1871, 1996.

[5] K. P. Koo and Wanser, A. D. Kersey, "Fibre laser sensor with ultrahigh strain resolution using interferometric interrogation", Electron. Lett., Vol. 31, pp. 1180–1182, 1995.

[6] J. T. Kringlebotn, "Optical fiber distributed feedback laser" (distributed feedback laser used as sensor), US Patent 5 844 927, UK Patent 2 299 203, NO Patent 302 441, Optoplan AS, 1996.

[7] T. Okoshi and K. Kikuchi, "Coherent optical fiber communications", (KTK Scientific Publishers, Tokyo, 1988), pp. 61–81.

[8] Y. Weissman, "Optical Network Theory", (Archtech House, 685 Canton Street, MA 02062, USA, 1992), pp. 142–152.

[9] H. L. An, E. Y. B. Pun, X. Z. Lin, and H. D. Liu, "Effects of Ion-Clusters on the Intensity Noise of Heavily Erbium-Doped Fiber Lasers", IEEE Phot. Technol. Lett., Vol. 11, pp. 803–805, 1999.

[10] F. Sanchez, P. Le Boudec, P. L. Francois, and G. Stephan, "Effects of ion pairs on the dynamics of erbium-doped fiber lasers", Phys. Rev. A, Vol. 48, pp. 2220–2229, 1993.

[11] J. Hübner, T. Feuchter, C.V. Poulsen, and M. Kristensen, "Directly UV-written erbium doped waveguides", in *Photosensitivity and Quadratic Nonlinearity in Glass Waveguides: Fundamentals and Applications*, OSA Technical Digest Series, Vol. 22, 1995.

[12] D. Marcuse, "Pulsed Behavior of a Three-Level Laser With Saturable Absorber", IEEE J. Quantum Electron., Vol. 29, pp. 2390–2396, 1993.

[13] K. E. Alameh, R. A. Minasian and Y. Zhao, "A Numerical Model for the Complex Susceptibility of Saturated Erbium-Doped Amplifiers", J. Quantum Electron., Vol. 33, pp. 855–860 (1997).

[14] E. Desurvire, "Study of the Complex Susceptibility of Erbium-Doped Fiber Amplifiers", J. of Lightwave Tech., Vol. 8, pp. 1517–1529, 1990.

[15] K. Petermann, "External optical feedback phenomena in semiconductor lasers", IEEE J. of Sel. Topics in Q. El., Vol. 1, pp. 480–487, 1995.

[16] G. A. Ball, C. G. Hull-Allen and J. Livas, "Frequency Noise of a Bragg grating fibre laser", Electron. Lett. **30**, 1229–*12*30 (1994).

[17] S. W. Løvseth, J. T. Kringlebotn, E. Rønnekleiv and K. Bløtekjær, "Fiber DFB Lasers Used as Acoustic Sensors in Air", Appl. Opt., Vol. 38, pp. 4821–4830, 1999.

[18] R. H. Kingston, "Detection of Optical and Infrared Radiation", (Springer-Verlag, Berlin, Germany, 1979), pp. 89–93.

[19] K. H. Wanser, "Fundamental phase noise limit in optical fibres due to temperature fluctuations", Electron. Lett., Vol. 28, pp. 53–54, 1992.

[20] W. H. Glenn, "Noise in Interferometric Optical Systems: An Optical Nyquist Theorem", IEEE J. Quantum Electron., Vol. 25, pp. 1218–1224, 1989.

[21] S. Knudsen, "Fiber-Optic Acoustic Sensors Based on the Michelson and Sagnac Interferometers: Responsivity and Noise Properties", Dr.ing. thesis, (Norwegian Univ. of Sci. and Tech. NTNU) 1996.

[22] K. H. Wanser, A. D. Kersey, and A. Dandridge, "Measurement of fundamental thermal phase fluctuations in optical fiber", in *Proceedings of 9th Optical Fiber Sensors Conference*, Florence, pp. 255–258, 1993.

[23] A. D. Kersey, "A Review of Recent Developments in Fiber Optic sensor Technology", Opt. Fiber Tech., Vol. 2, pp. 291–317, 1996.

[24] M. K. Davis, M. J. F. Digonet, and R. H. Pantell, "Thermal Effects in Doped Fibers", J. of Lightwave Tech., Vol. 16, pp. 1013–1023, 1998.

[25] O. Hadeler, M. N. Zervas, E. Rønnekleiv, and M. Berendt, "Temperature distribution along DFB fibre lasers", *IEE colloquium digest on Optical Fibre Gratings*, (IEE, Box 96, M. Faraday House, Stevenage, Herts. SG1 2SD, UK), 1999.

[26] M. Kuorogi, C. H. Shin, and M. Ohtsu, "A 250 Hz Spectral Linewidth 1.5 μm MQW-DFB Laser Diode with Negative-Electrical-Feedback", IEEE Phot. Tech. Lett., Vol. 3, pp. 496–498, 1991.

[27] G. A. Ball, G. Hull-Allen, C. Holton, and W. W. Morey, "Low Noise Single Frequency Linear Fibre Laser", *Electron. Lett.*, vol. 29, pp. 1623-1625, 1993.

[28] V. Mizrahi, D. J. DiGiovanni, R. M. Atkins, S. G. Grubb, Y.-K. Park, and J.-M. P. Delavaux, "Stable Single-Mode Erbium Fiber-Grating Laser For Digital Communication", J. of Lightwave Tech., Vol. 11, pp. 2021–2025, 1993.

[29] J. Hübner, P. Varming and M. Kristiansen, "Five wavelength DFB fiber laser source for WDM systems", *Electron. Lett.*, vol. 33, pp. 139-140, 1997.

[30] K. P. Koo and A. D. Kersey, "Noise and cross talk of a 4-element serial fiber laser sensor array", in *1996 Conf. on Optical Fiber Communications*, paper ThP2, Tech. Dig., pp. 266-267.

Chapter 4

Stability of Distributed Feedback Fiber Lasers with Optical Feedback[1]

Abstract — The tolerance of two fiber distributed feedback lasers to external back-reflection from discrete reflectors and to Rayleigh back-scattering has been investigated. The results show a reduced feedback sensitivity for the longer laser grating.

4.1 Introduction

Fiber distributed feedback (DFB) lasers used as sensor elements with optical frequency interrogation is an attractive high resolution alternative to passive Bragg grating sensors. Remote pumping and interrogation of such sensor lasers without the use of an optical isolator near the sensing point may be required. However, this will introduce Rayleigh back-scattering into the laser from the lead fiber. If in addition several laser sensors at different wavelengths are serially multiplexed along the same fiber [1], each laser may also experience discrete external reflections from the grating side-bands of the other lasers.

It is known that back-reflections into narrow linewidth semiconductor lasers may cause increased frequency noise, or even self pulsing. The tolerable back-reflection level of such lasers has been found to decrease with increasing external cavity length and with decreasing laser mirror reflectivity [2]. However, important laser parameters such as the frequency and relative linewidth (inverse Q-value) of the relaxation oscillation resonance and the coherence length

[1]This chapter contains a re-edited version of [E. Rønnekleiv and S. W. Løvseth, "Stability of Distributed Feedback Fiber Lasers with Optical Feedback", in *13th International Conference on Optical Fiber Sensors*, Proceedings of SPIE Vol. 3746, pp. 466-469, 1999].

of the solitary laser differ largely, typically by orders of magnitude, between semiconductor lasers and fiber DFB lasers. Therefore, few quantitative conclusions can be made about the back-reflection tolerance of fiber DFB lasers from existing work on semiconductor lasers.

In this paper we investigate the feedback attenuation required for stable operation of Er^{3+} fiber DFB lasers experiencing Rayleigh back-scattering or discrete end-reflection from fiber lengths ranging from $\sim$ 10 m to 13 km. We also discuss the possibility of improving the tolerance to back-reflections by increasing the DFB grating strength and/or by using a laser with asymmetric output characteristics.

4.2 Experiments and Results

Two Er^{3+} doped fiber DFB lasers, made by IONAS, Denmark, with grating lengths of 5 and 10 cm and nominal $\pi/2$ phase-shifts at the grating center have been investigated. In the following they will be denoted DFB1 and DFB2, respectively. From a heat scan measurement [3], the coupling coefficients were estimated to $\kappa = 170$ m^{-1} for DFB1 and $\kappa = 150$ m^{-1} for DFB2, giving total grating strengths of $\kappa l = 8.5$ and 15, respectively. Fundamental mode operation at the Bragg resonance frequency was verified for DFB1, while it was found that DFB2 could switch from the fundamental to a higher order longitudinal mode, depending on how the fiber was mounted. The higher order mode of DFB2 was found to be highly asymmetric, with a 15.8 dB ratio between the left and the right output power. When operating in the fundamental mode this ratio was 0.9 dB for DFB1 and 6.0 dB for DFB2. Both lasers were operating in only one polarization mode, and the laser wavelengths were 1551.1 nm for DFB1 and 1554.6 nm for DFB2.

The experimental setup is shown in Figure 4.1. The fiber laser was pumped at 1480 nm from the left through a 1480/1550 wavelength division multiplexer (WDM). Both lasers were pumped through their high output power ends. The output from the 1550 branch of the WDM was guided through a 50 dB optical isolator (ISO) and split by a 3 dB coupler, enabling the fiber laser frequency and the output power from the left to be measured simultaneously. The frequency was measured using a Mach-Zender interferometer (MZ), having an imbalance of 101.5 m and fringe sensitivity of 321 kHz/rad. A polarization controller (PC2) was used to optimize the interferometer response, and quadrature operation was ensured by feedback from the differential detector (D1 and D2) to a PZT stretcher inside the interferometer through a low-pass filter (LPF). The laser output power to the left was measured with detector D3, and was kept at 121 μW for DFB1 and 313 μW for DFB2 during all the experiments. The relative intensity noise (RIN) and frequency noise of the lasers without

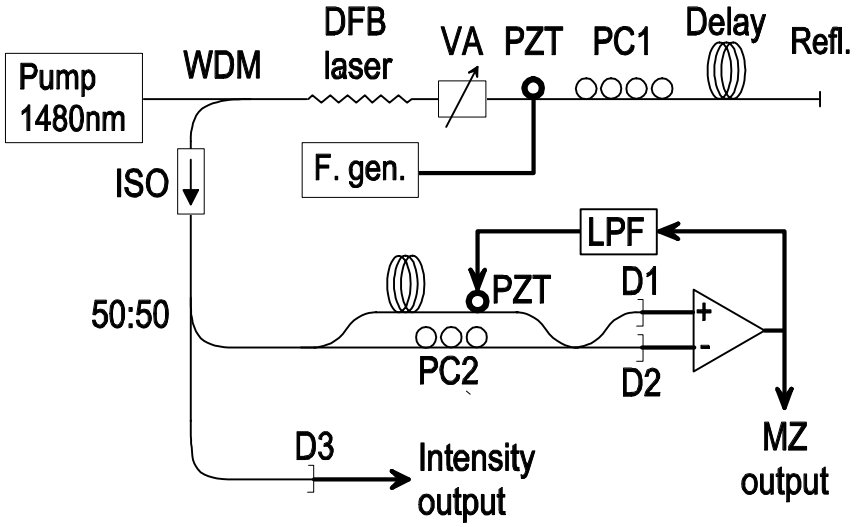

Figure 4.1. Experimental setup for investigation of DFB fiber lasers with optical feedback.

back-reflection in the frequency range from 2.4 to 930 kHz were measured to be 5.6 kHz and -36 dB (RMS values) for DFB1 and 6.5 kHz and -43 dB for DFB2. The 3 dB bandwidth and center frequency of the relaxation oscillations were roughly 8 kHz and 207 kHz for DFB1 and 18 kHz and 238 kHz for DFB2, respectively.

The right end of the fiber laser was connected through a variable optical attenuator (VA) to various fiber delay coils, ranging in length from a few meters to 13 km. By terminating the ends of the delay coils with bending losses, the effect of Rayleigh back-scattering at different attenuator settings could be investigated. To study the effect of back-reflection from a discrete point, we used a mirror with -0.75 dB reflectivity or a -14.5 dB cleaved fiber end reflector. The PZT phase modulator and the polarization controller (PC1) were used to control the phase and polarization of the feedback signal. Standard telecom fiber of varying fabricates were used in the delay coils, and the back-scattered Raleigh power per unit length may have varied by ± 1 dB between the coils. The lengths and transmission losses were measured with an OTDR. Connector and splice losses were measured, and have been included in the stated attenuation values.

For Rayleigh scattering, one important parameter is the length of back-scattering fiber the laser can tolerate before the noise induced by back-reflection start to dominate over other noise sources. For longer lengths, it is interesting to know the attenuation required to maintain stable operation. The RMS frequency noise of DFB1 seemed unchanged for fiber lengths up to 37 m, but at 142 m the laser was self pulsing with excessive frequency noise. The noise of

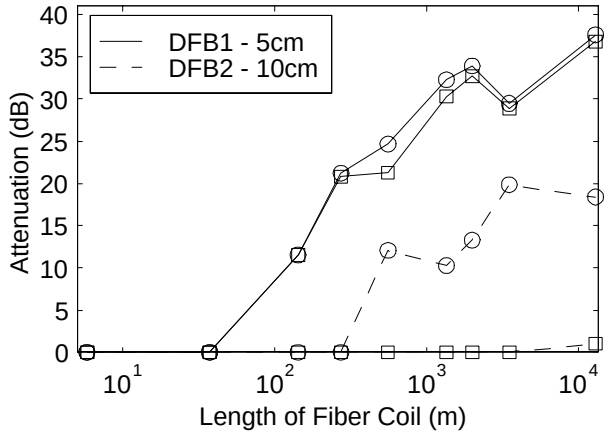

Figure 4.2. Attenuation needed for stable operation in frequency and intensity of DFB1 and DFB2 exposed to Raleigh scattering from fiber delay as a function of delay lengths. Curves with square markers (□) show the smallest attenuation measured to get CW operation (see main text), whereas curves with circular markers (◯) show the smallest attenuation needed for max. ±20 kHz relaxation oscillation amplitude.

DFB2 seemed unchanged for lengths up to 273 m. With 13 km of fiber, RMS noise of 37 kHz with bursts of ±170 kHz could be observed. We also measured the attenuation needed between the delay fiber and the DFB fiber lasers to avoid frequency noise bursts with amplitudes exceeding ±20 kHz during a period of 12 s and the attenuation needed for continuous wave (CW) operation for the same duration. By CW operation we mean that the intensity should not have any noise with amplitude larger than 30 % of the DC value.

The results of the Rayleigh measurements are displayed in Figure 4.2. As seen from the figure, DFB2 is considerably more stable than DFB1 for fiber lengths above 100 m. At 13 km, the attenuation needed to avoid excess noise with DFB1 was 19.2 dB higher than with DFB2. DFB2 was only showing small signs of self oscillation at 13 km delay, with only 0.5 dB attenuation required for CW operation. DFB1, on the other hand, started self-oscillations for attenuation levels only slightly below those where the frequency noise started to increase, and at 13 km delay, 36.7 dB attenuation was needed for CW operation. Also note that the attenuation needed seems to approach saturation for the longest fiber delays from 2 to 13 km. This is expected, since the Rayleigh scattering feedback per fiber length levels will be lower far away from than close to the laser due to the fiber transmission losses. In addition, the longest lengths correspond to several relaxation oscillation periods [2].

As discussed by Petermann [2] and others, a discrete reflector will shift both the intensity, frequency, and linewidth of the laser, depending on the phase of the back-reflection. In a real sensor application, the phase of back-reflections

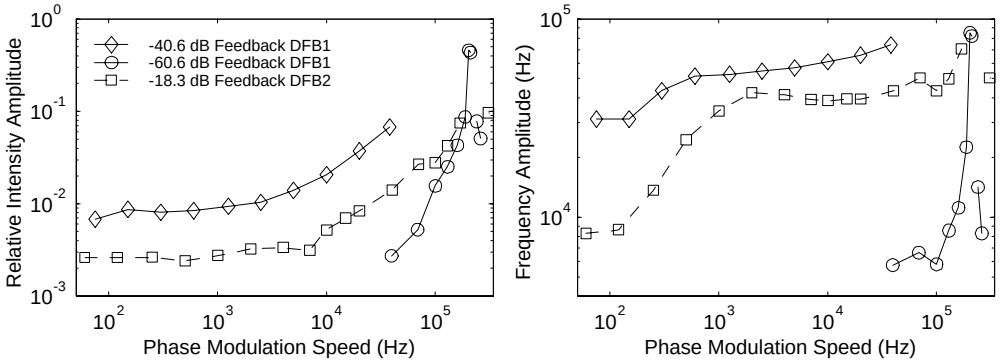

Figure 4.3. Laser intensity (left) and frequency (right) response as a function of phase modulation frequency of feedback from a distance of 28.5 m (DFB1) and 29.5 m (DFB2).

may drift at various speeds due to mechanical vibrations in the lead fiber. It is thus interesting to investigate how the laser frequency and intensity amplitudes vary with the phase modulation speed. Setting PC2 to the position of largest possible response, we measured this frequency response for a distance between the reflector and the fiber lasers of 29 meter. Phase modulation was obtained by driving the PZT ring in the delay with a triangular waveform. For phase modulations speeds far below the relaxation oscillation frequencies, this produced fringes in the laser frequency and intensity which easily could be measured with an oscilloscope. For larger phase modulation speeds, large relaxation oscillations were triggered and we had to estimate the frequency response from the Fourier spectra of the oscilloscope traces. The results are shown in Figure 4.3. Note that different feedback levels were used in the measurements, and that DFB1 starts to self-oscillate for modulation speeds close to the relaxation oscillation peak even at a feedback level less than -60 dB.

Similar to the Raleigh scattering case, we measured the largest feedback with less than 6 dB worst case increase in RIN, with less than $\pm$20 kHz relaxation oscillation amplitude, and with CW laser operation. The two latter results are shown in Figure 4.4. The phase of the feedback was again modulated with the PZT, yielding comparable noise bursts at each fringe. The figure shows the feedback level for a phase modulation speed of 1 and 10 kHz for the frequency noise and 1 kHz for the CW limit measurements. The largest feedback levels for 10 kHz are slightly larger than for 1 kHz. The explanation is probably that the laser in the former case are shorter period of time in the unstable regime. The tolerable feedback seems to approach constant levels for delays longer than one relaxation oscillation period, corresponding to a fiber delay of roughly 500 m. This is in agreement with the theory for semiconductor lasers [2].

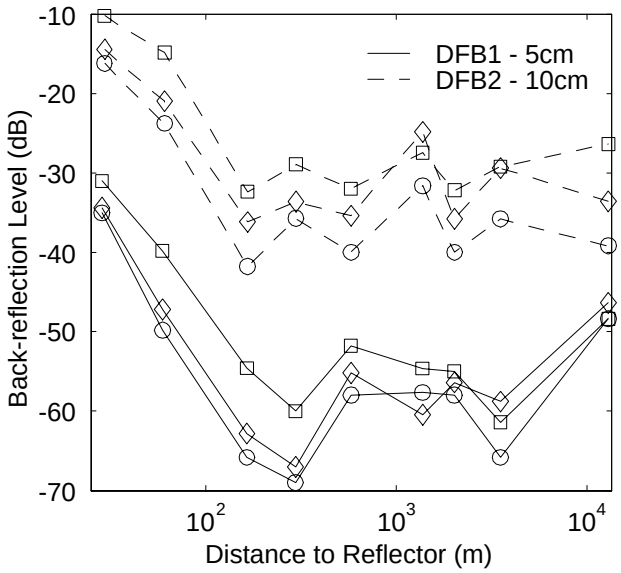

Figure 4.4. Maximum feedback allowed from discrete reflectors for stable operation in frequency and intensity of DFB1 and DFB2. Curves with circular (◯) and square (□) markers show the largest feedback allowed to get a maximum relaxation oscillation amplitude of ±20 kHz for a back-reflection phase modulation speed of 1 and 10 kHz, respectively. Curves with diamond (♢) markers show maximum feedback allowed for CW operation for a back-reflection phase modulation speed of 1 kHz.

4.3 Conclusion

We see from the measurements that the 10 cm DFB2 with $\kappa l \approx 15$ can tolerate back-reflection levels that are about 20 dB higher than the 5 cm DFB1 with $\kappa l \approx 8.5$. This is believed to be due to a weaker coupling of the laser modal power of DFB2 to the external cavity [2]. Since the longitudinal mode of operation in this laser during the experiment is not known, clear conclusions cannot be made about the reason for this weak coupling. If DFB2 was operating in its fundamental mode, an important reason is probably the increased intensity concentration near the phase-shift position for higher κl values [3]. In theory, an increase in κl by 6.5 corresponds to a reduction in coupling efficiency by $e^{-6.5}$, and the tolerable back-reflection level should thus be increased by $20\log_{10}(e^{6.5}) = 56$ dB.[2] Not included in this estimate are possible effects of non-linearities due to the high intensity inside high κl lasers, which may contribute to a reduced stability.

[2] In the conference proceding we wrote that the tolerable back reflection level is increased by 28 dB, which is wrong.

If DFB2 has been operating in the higher order mode, the improved tolerance to back-reflection should rather be explained by the 16 dB output asymmetry of this mode. This corresponds to an external cavity coupling coefficient that is 16 dB lower to the left than to the right, and the tolerable feedback level should thus be higher by 16 dB at the right side. In principle, asymmetric output lasers could be exploited by mounting the laser with the low output end pointing towards the source of back-reflections, i. e. the lead fiber. The expense of such a solution would be a reduced output power returned through the lead fiber.

The maximum length of Rayleigh back-scattering fiber that would give no excess noise without attenuation was found to be around 100 m for DFB1 and around 300 m for DFB2. DFB2 can however be made free from excess noise for all the investigated fiber lengths up to 13 km by introducing a 10 dB attenuator at the laser wavelength near the laser. Again, this would give a 10 dB reduction in output power.

References

[1] K. P. Koo and A. D. Kersey, "Noise and cross talk of a 4-element serial fiber laser sensor array", 1996 Conf. on Optical Fiber Communications, paper ThP2, Technical Digest, pp. 266-7.

[2] K. Petermann, "External optical feedback phenomena in semiconductor lasers", IEEE J. of Sel. Topics in Q. El., Vol. 1, pp. 480-7, 1995.

[3] E. Rønnekleiv, M. Ibsen, M. N. Zervas and R. I. Laming, "Characterization of intensity distribution in symmetric and asymmetric fiber DFB lasers", CLEO'98, Tec. Digest Vol. 6, CTuE6, (San Francisco), 1998.

Chapter 5

Stability of an Er–Yb-doped fiber distributed-feedback laser with external reflections[1]

Abstract — The maximum tolerable amplitude backreflection coefficient $r_{ext,c}$ into a fiber distributed feedback (DFB) laser before the onset of instabilities has been investigated. $r_{ext,c}$ was found to decrease with increasing external cavity lengths up to ∼320 m and to be proportional to the relative linewidth of the relaxation oscillation resonance. The tolerable length of Rayleigh backscattering standard telecom fiber was found to be 135-200 m. An observed degradation in the laser stability and slope efficiency at low pump powers is believed to be due to UV-induced saturable absorbers.

5.1 Introduction

Fiber distributed-feedback (DFB) lasers are attractive used as sensor elements with optical frequency interrogation because of their low level of frequency noise[2] and stable longitudinal mode operation. Remote pumping and interrogation of such sensor lasers through a long lead fiber may be required. For operational reasons, the use of optical isolators near the sensing point may be undesirable. Consequently, the laser will experience Rayleigh back-scattering from the lead fiber. If in addition several sensor lasers at different wavelengths

[1]This chapter contains a re-edited version of [E. Rønnekleiv, O. Hadeler, and G. Vienne, "Stability of an Er-Yb-doped fiber distributed-feedback laser with external reflections", Opt.. Lett., Vol. 24, pp. 617-619, 1999].

[2]"low-frequency noise" in the original paper has been corrected to "low level of frequency noise"

are serially multiplexed along the same fiber [1], each laser may also experience reflections from the grating side-bands of the other lasers. It is known that external backreflections can cause excess frequency noise or even self-pulsing in narrow linewidth semiconductor lasers [2]. This problem increases with decreasing laser mirror reflectivity and with increasing distance to the external reflector. However, important parameters such as the optical coherence lengths and the relaxation oscillation resonance Q-factors and center frequencies differ largely between semiconductor lasers and fiber DFB lasers. Therefore, few quantitative conclusions can be made about fiber DFB laser stability from existing work on semiconductor lasers.

5.2 Experiment

In this Letter we report on the tolerance of an Er–Yb-doped fiber DFB laser to external backreflections. The investigated laser operated at 1549 nm in two polarization modes and was pumped by a 1480-nm laser diode. We produced laser operation by writing a symmetric π phase-shifted grating of length L =40 mm into a UV-sensitized B–Ge doped ring enclosing the Er–Yb doped core of the fiber [3]. D_2-loading was used to enhance the UV-sensitivity. The grating coupling coefficient of the laser was measured by a heat-perturbation method [4] to be κ =230 $m^{-1}\pm10\%$. Before UV exposure but after D_2-loading of the fiber, the fiber transmission spectrum was measured for various pump powers. From these measurements, the absorption (a_x) and gain (g_x) at zero and full inversion, respectively, at the laser signal ($x = s$) and pump ($x = p$) wavelengths were found to be $[\, a_s,\, a_p, g_s,\, g_p] = [11.7,\, 8.9,\, 15.9,\, 3.0]$ dB/m. The spontaneous emission power at full inversion was $P_{sp} = 4.1$ mW/m.

Figure 5.1 shows the measured left + right output power (crosses) emitted from the laser versus pump power. Curve A shows the theoretical output power, obtained from the measured gain parameters of the unexposed fiber and a DFB laser model described elsewhere [5]. The measured slope efficiency increases at low pump power and approaches a constant value of 0.7% above 40 mW. This indicates that bleachable absorbers are present which saturate for pump powers of >40 mW. We obtained a good theoretical fit (curve B) by assuming a lifetime reduction ("quenching") by a factor of $\zeta = 26$ for a fraction $\xi = 37.7$ % of the Er-ions, and unbleachable losses of $a_0 = 0.243$ dB/m. Here, ξ is essentially determined by the laser threshold, ζ by the position of the "knee" in the output power curve near 30 mW and a_0 by the slope efficiency at high pump powers.

It may be noted that higher slope efficiencies (>10%) could be obtained by pumping at 980 nm. However, the high pump absorption per laser in this case makes serial sensor multiplexing impossible. Moreover, the increased heat dissipation from the laser may disturb the sensor performance. For accurate

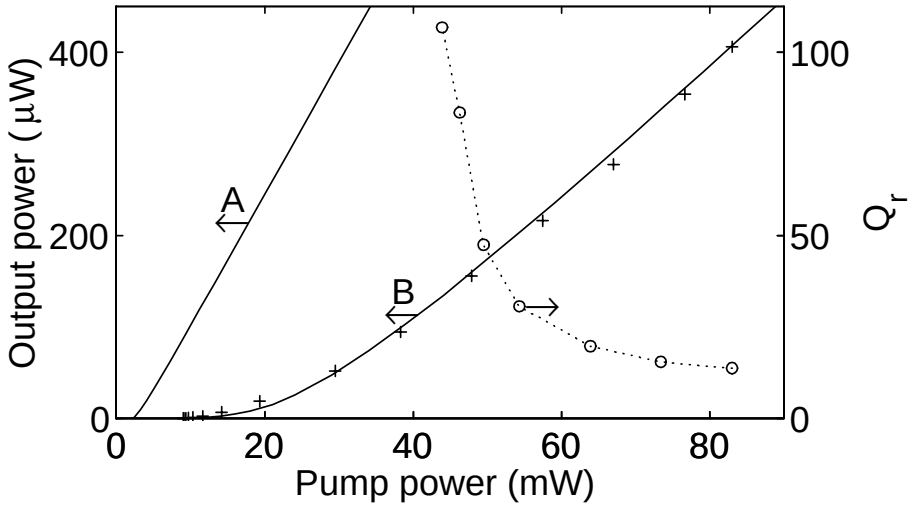

Figure 5.1. Measured laser output power (crosses) and relaxation oscillation Q factor Q_r (circles) versus pump power. Solid lines, theoretical output power assuming that A, $\xi = 0$, $a_0 = 0$; B, $\xi = 37.7\%$, $\zeta = 26$, $a_0 = 0.243$ dB/m.

interrogation of the laser as a sensor, the output power obtained with 1480 nm pumping is more than sufficient.

Before UV exposure the loss saturation versus bleaching power was measured for the laser fiber at 1535 nm. Parameter fitting to these measurements shows that less than $\xi_{\max} = 5$ % of the Er-ions were quenched by the factor $\zeta = 26$. The unbleachable losses were limited to $a_0 < 0.3$ dB/m. Moreover, the transmission spectrum versus pump power measurements show that the effective value of ξ does not vary significantly between 1535 nm and 1549 nm. Consequently, the majority of the bleachable absorbers seem to have been introduced during the UV exposure.

The relaxation oscillation resonance Q factor $Q_r = f_r/\Delta f_r$ of the solitary laser was also measured, and is shown by the open circles in Figure 5.1. Here, f_r is the peak frequency and Δf_r the 3-dB peak width of the intensity noise spectrum. Below a pump level of 40 mW the laser was self pulsing. Above 40mW a steep reduction in Q_r was observed, parallel with the bleaching of the UV-induced absorbers. It is known that bleachable absorbers can cause laser instabilities [6], and we believe that the bleachable absorbers play an important role in reducing the stability of the investigated laser at low pump powers. f_r followed a nearly linear dependence ($\pm$1.5 kHz) on the pump power from f_r=109 kHz at 42 mW to f_r=207 kHz at 83 mW.

Figure 5.2 shows the setup that we used to study the effects of backreflections. The laser was pumped from the left, and the left output power was guided

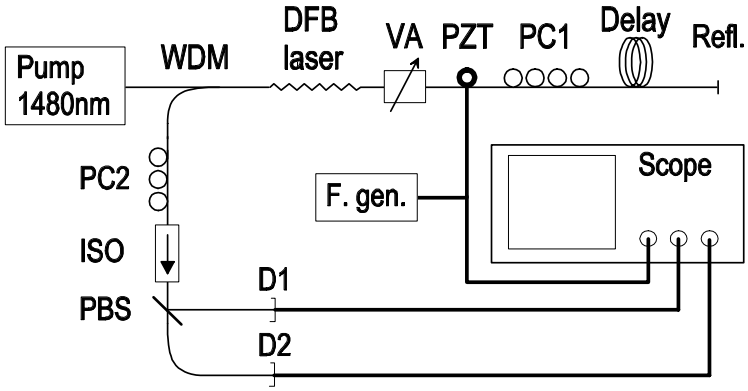

Figure 5.2. Setup for study of backreflection-induced self-oscillations: F.gen., function generator.

through a wavelength division multiplexer (WDM), a polarization controller (PC2), an isolator (ISO) and a polarization beam splitter (PBS) to detectors D1 and D2. PC2 was adjusted such that each detector received light from only one laser polarization mode. Backreflection into the right-hand end of the laser with variable attenuation, phase shift, polarization shift and delay was generated by use of a variable attenuator (VA), a piezoelectric fiber stretcher (PZT), a polarization controller (PC1) and a selection of delay coils with -14.5 dB cleaved end reflectors (Refl.).

With an external cavity length of $L_{ext} = 22.3$ m and a pump power of 83 mW, the effective external reflection coefficient r_{ext} seen by the laser was first adjusted to its critical value, $r_{ext,c} = -28.3 \pm 1$ dB, where relaxation oscillation noise bursts started to occur for worst-case settings of PC1 and the PZT voltage. By "worst-case" we mean that the noise amplitude was at its maximum. Figure 5.3 shows the evolution of the left output power P_{left} from the laser (recorded by D1 + D2) when the PZT was driven by a triangular waveform. The round-trip phase modulation ϕ_{ext} induced by the PZT is also shown in the figure. The periodic relaxation oscillation noise bursts are believed to be related to mode hopping or to unstable regimes at the transitions between external cavity modes [2]. For higher backreflection levels the laser was continuously self-pulsing. The deterministic dependence of P_{left} on ϕ_{ext} is believed to be due to a modulation of the effective right-hand mirror reflectivity of the laser.

When PC1 was in its worst case position, the power fluctuations of the two laser polarization modes were practically equal and in phase. This indicates equal backreflection phase shifts for the two polarizations. For other settings of PC1, the fast relaxation oscillations of the two polarizations would still be in phase, but the sign of the deterministic power oscillations could be made

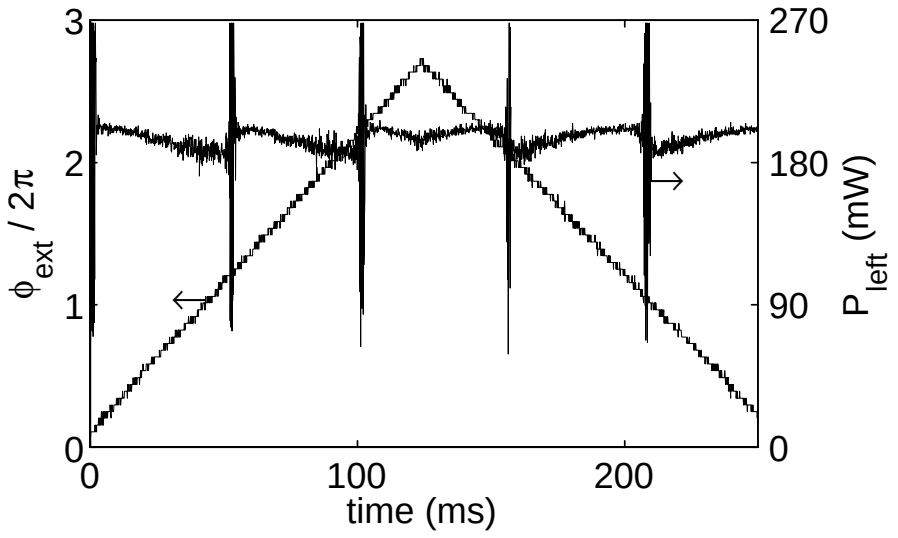

Figure 5.3. Scope traces of the left-hand output laser power P_{left} and of the phase modulation signal ϕ_{ext} applied to the PZT. $L_{ext} = 22.3$ m and $r_{ext} = r_{ext,c}$.

opposite for the two modes. For moderate phase modulation speeds ($d\phi_{ext}/dt <$ 5 rad/ms), $r_{ext,c}$ could be increased by at least 10 dB by adjustment of PC1. However, control of the reflected polarization to ensure stability is believed to be unrealistic in most real applications.

Figure 5.4 shows $r_{ext,c}$ measured for nine different combinations of L_{ext} and pump power, with worst-case settings of PC1. Simulation results reported for semiconductor lasers [7] show that $r_{ext,c}$ versus L_{ext} decreases steeper than -20 dB per decade for $L_{ext} < L_r = c/2nf_r$, and flattens out for longer lengths. Here, L_r corresponds to a feedback delay of one relaxation oscillation period, c being the speed of light in vacuum and n the refractive index of the fiber. The results in Figure 5.4 are in qualitative agreement with the simulations.

For L_{ext} =22.3 and 318 m the measurements satisfy $r_{ext,c} \propto Q_r^{-1}$ to within ± 0.6 dB. This is expected, as it can be shown that the phase stability margin of the intensity feedback loop that causes the relaxation oscillation resonance of the solitary laser equals Q_r^{-1} (rad). For L_{ext} =1518 m the deviations from $r_{ext,c} \propto Q_r^{-1}$ are larger. This may be related to variations in the relaxation oscillation phase $\Phi = 2\pi L_{ext}/L_r$ of the external feedback when L_r changes (c.f. table in Figure 5.4).

The feedback parameter [2, 7] C can be written for a DFB laser as

$$\begin{aligned} C &= \sqrt{1+\alpha^2}\frac{2L_{ext}}{L_L}\,T_2\,r_{ext} \\ &= \sqrt{1+\alpha^2}\,4\kappa\exp(-\kappa L)L_{ext}r_{ext}, \end{aligned} \tag{5.1}$$

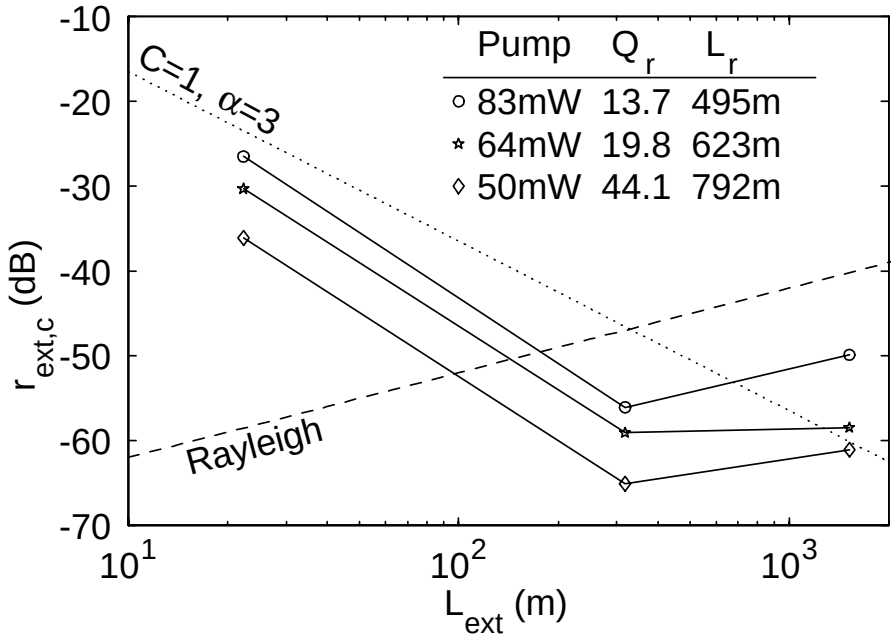

Figure 5.4. Measured critical external reflection coefficient $r_{ext,c}$ for several external cavity lengths L_{ext} and pump powers.

where $L_L = 2/\kappa$ is the effective round-trip path length of the laser, L the DFB-grating length, $T_2 = 4\exp(-\kappa L)$ is the power transmission coefficient of the right half of the grating, $\alpha = d\chi'/d\chi''$ the linewidth broadening factor and $\chi = \chi' + i\chi''$ the complex susceptibility of the gain medium. The limit $C = 1$ when assuming $\alpha = 3$ is shown in Figure 5.4. Below this line, only one external cavity mode solution will exist for any value of ϕ_{ext}, and mode-hopping cannot occur. Still, unlike the findings for semiconductor lasers [2, 7], self oscillations were observed for the laser that we investigated in this regime. This may partly be due to errors in the estimates for α and κ, which may cause significant errors in C. Moreover, it is believed that high-Q_r lasers like the one investigated can become unstable even for $C < 1$. This is because the laser stability margin Q_r^{-1} will be somewhat modified by the backreflection.

Simulation results reported for an Er-doped amplifier [8] indicate that α is proportional to the signal to saturation power ratio P_s/P_{sat}, approaching $\alpha \sim 3$ for $P_s/P_{sat} = 20$. For our laser an effective ratio $4 < P_s/P_{sat} < 20$ is estimated, depending heavily on the $\pm 10\%$ error margin of κ. Thermal effects may also contribute to the effective value of α, as the refractive index depends on the laser power through self-heating of the cavity.

We tested the tolerance to Rayleigh back-scattering by disconnecting the variable attenuator and splicing a coil with standard telecom fiber to the right-hand laser output. The coil end was terminated with bending losses. For 83-mW pump the laser was found to be stable with Rayleigh scattering from $\leq$135 m of fiber. At 135 m noise bursts could be observed in response to severe acoustical noise, such as clapping hands in the laboratory. Bursting or continuous self oscillations were observed for lengths of $\geq$200 m. The dashed line in Figure 5.4 corresponds to a typical Rayleigh back-scattering level of -72 dB/m. The cross-over point between this line and the straight line interconnecting the discrete reflection measurements is at 175 m, which is in good agreement with the Rayleigh measurements.

5.3 Conclusion

In conclusion, we have found that $r_{ext,c}$ has a proportional dependence on the stability margin Q_r^{-1} of the solitary laser, and decreases with increasing external cavity length for $L_{ext} < L_r$. Both the stability margin and the slope efficiency of the laser were found to decrease dramatically at pump powers below 60 mW. This is believed to be related to saturable absorbers introduced during the UV-exposure. The laser frequency noise was not measured in the present experiment. However, recent backreflection studies of similar fiber DFB lasers [9] have shown that the occurrences of excess frequency and intensity noise are highly correlated. One way of improving the tolerance to backreflections may be by increasing κL, as indicated by Eq. (5.1). There is, however, a limit to how high κL can be made before the laser tends to operate in higher order longitudinal modes [4]. Moreover, the effective value of α may increase as the intensity inside the cavity increases with κL, contributing to a reduced backreflection tolerance.

The authors acknowledge Morten Ibsen for providing the DFB grating for this experiment. The experimental part of this work was performed while all three authors were with the Optoelectronics Research Center in Southampton. E. Rønnekleiv acknowledges support from his employer Optoplan AS, the Norwegian Research Council and British Council. O. Hadeler acknowledges support through a CASE award from BICC plc, UK.

References

[1] K. P. Koo and A. D. Kersey, 1996 in *Optical Fiber Communications Conference (OFC)*, Vol. 2 of 1996 OSA Technical Digest Series (Optical Society of America, Washington, D.C., 1996), paper ThP2.

[2] K. Petermann, IEEE J. of Sel. Topics Quantum Electron., **1**, 480 (1995).

[3] L. Dong, W. H. Loh, J. E. Caplen, J. D. Minelly and L. Reekie, Opt. Lett., **22**, 694 (1997).

[4] E. Rønnekleiv, M. Ibsen, M. N. Zervas and R. I. Laming in *Conference on Lasers and Electro-Optics (CLEO)*, Vol. 6 of 1998 OSA Technical Digest Series (Optical Society of America, Washington, D.C., 1998), paper TuE6.

[5] E. Rønnekleiv, M. N. Zervas and J. T. Kringlebotn, IEEE J. Quantum Electron., **34**, 1559 (1998).

[6] D. Marcuse, IEEE J. Quantum Electron., **29**, 2390 (1993).

[7] N. Schunk and K. Petermann, IEEE Photon. Technol. Lett., **1**, 49 (1989).

[8] K. E. Alameh, R. A. Minasian and Y. Zhao, J. Quantum Electron., **33**, 855 (1997).

[9] E. Rønnekleiv and S. W. Løvseth, "Stability of Distributed Feedback Fiber Lasers with Optical Feedback", in *13th International Conference on Optical Fiber Sensors*, Proceedings of SPIE Vol. 3746, pp. 466-469, (1999).